THESIS

EFFECTS OF WARMING AND STRATOSPHERIC AEROSOL INJECTION ON TROPICAL CYCLONE DISTRIBUTION AND FREQUENCY IN A HIGH-RESOLUTION GLOBAL CIRCULATION MODEL

Submitted by

Andrew Feder

Department of Atmospheric Science

In partial fulfillment of the requirements

For the Degree of Master of Science

Colorado State University

Fort Collins, Colorado

Fall 2024

Master's Committee:

Advisor: David Randall

James Hurrell
Jeremy Rugenstein

ABSTRACT

EFFECTS OF WARMING AND STRATOSPHERIC AEROSOL INJECTION ON TROPICAL CYCLONE DISTRIBUTION AND FREQUENCY IN A HIGH-RESOLUTION GLOBAL CIRCULATION MODEL

Tropical cyclones (TCs) occur stochastically in any given TC season, with varying numbers and intensities within basins over time. Nevertheless, they arise out of fundamental laws of thermodynamics and fluid physics, and in recent years, as global circulation models (GCMs) have increased in spatial resolution, increasingly realistic TCs and TC distributions have emerged from them. Where prior research on TC climatologies has relied on proxies like Potential Intensity (PI) and synthetic storm models, the cyclones emerging from the dynamics of newer GCMs can now be analyzed directly, using native model variables.

Such direct analysis may be particularly useful in studying possible global storm distributions under radically altered future climates, including high-emissions warming scenarios, and even those shaped by climate interventions. These interventions include various directed changes in global albedo, such as Stratospheric Aerosol Injection (SAI), with only limited precedent in the historical period.

GCMs simulating realistic climate intervention scenarios, have not as of yet paired storm-resolving resolution with realistic intervention scenario construction. This has left gaps in our understanding as to how interventions might affect global storm/TC distributions, and whether ameliorating warming in this way could also substantially lessen related natural disaster risk profiles.

In this paper, we utilize a new high-resolution model configuration to conduct experiments examining the effects of SAI, on tropical cyclones and global storm physics more broadly. These experiments are constructed based on prior work on SAI using the GLENS GCM ensemble (Tilmes et al. 2020; Danabasoglu 2019a,b). Our analysis centers on 3 10-year experiments conducted using 30-km grid spacing. These include a recent-past calibration run; the Intergovernmental Panel on Climate Change climate pathway SSP 8.5 (IPCC 2021), for the years 2090-2099, with no SAI; and SSP 8.5, with SAI having begun in 2020 to maintain a global temperature rise of no more than 1.5° C, also simulated for the years 2090-2099. With the resulting data sets, we deploy a novel TC-tracking algorithm to analyze resulting changes in storm tracks and properties. Based on our results for these different scenarios, we find that SAI, while in

some ways restoring global storm patterns to a pre-warming state, may also create unique basin-scale TC distribution features and pose novel related hazards.

ACKNOWLEDGMENTS

The research presented here was made possible with the help of many friends and colleagues at CSU and beyond. Foremost among them are my advisor, David Randall, and my fellow research group member Donald Dazlich. Through their conversation, advice, encouragement, and critical assistance they have enabled me to overcome all manner of unexpected technical challenges and road bumps on this project.

The advice of John Knaff and Christopher Slocum have been invaluable in understanding the large-scale conditions that lead to TC development, and for broadly helping me reach fluency in the techniques used to analyze cyclogenesis favorability. They and Yushan Han at UC Davis, prompted me to reconsider our persistent sub-tropical cyclone misidentification issue, and pointed me toward possible solutions and important limitations of TC tracking algorithms more broadly. Michael Bell, over the course of many meetings was incredibly helpful in deciding on metrics to use in analyzing possible future climates and in understanding how TCs fit into the broader climate system.

James Hurrell played a very important role at the idea stage of this thesis, nudging all of us toward a set of experiments and scientific questions more in line with what was feasible, and what was salient.

I would like to thank my family, in particular my mother Jody, who has been a rock over the whole tumultuous period of bringing this project to fruition, occurring as it did alongside a host of life transitions and other graduate school challenges. And I would like to thank all the new friends I've made here in Fort Collins, for helping me build a new life here, and helping me feel like I truly belong.

This has been maybe my greatest endeavor so far, but I have big plans for the future and I look forward to having you all with me on the journey to come.

TABLE OF CONTENTS

LIST OF FIGURES

CHAPTER 1

INTRODUCTION

1.1 TCs, PAST AND FUTURE

Tropical cyclones (TCs) can be understood as Carnot engines (Emanuel et al. 2023) powered by heat energy from the ocean surface. As such, their occurrence is highly connected to heat and its movement. Fundamentally, TCs are a mechanism by which the atmosphere transfers heat from the ocean to the upper atmosphere, with other features such as intense cyclonic winds, rain bands, etc, arising from this transfer and thus ultimately fueled by this energy differential. Yet, TCs do not appear wherever they could perform this function, and in fact potentially represent a very small share of the relevant heat transfer budgets (Emanuel 2022). Rather, TC occurrence is dependant on a host of other variables being conducive to their formation and survival, and overall storm activity is thus much harder to predict than if it were primarily a function of available energy. As well, over shorter periods TC populations are highly influenced by chance, linked to the random distribution of seeding events occurring in conjunction with these storm ingredients to take shape into realized cyclones.

As TCs arise stochastically and as a highly contingent, emergent phenomenon, it is difficult to draw direct inferences about changes in TC behavior from long-term climate trends. For purposes of this project, TCs are defined as cyclonic storms with maximum sustained winds of 33+ m/s, categories 1-5, with weaker systems exhibiting tropical storm (TS) and tropical depression (TD) intensity. The statistically small number of TCs that comprise an annual season (∼50 a year category 1+ in IBtRACS global best-track data spanning 2010-2019) (Knapp et al. 2010, 2023)), further create a large barrier to establishing meaningful trends in the recent historical record. Over longer time scales, paleotempestological proxy records too remain fairly limited in scope, number and resolution. Such geologic records inherently pertain to small localized areas, and do not reveal prior storm trajectories or overall regional/global distributions (Benton et al. 2022).

The ultimate result of all these epistemological limitations is a dearth of good observational information about how TCs have historically interacted with climate. The era of fairly complete global observational TC records begins ∼1990 (Klotzbach et al. 2022), and spans a period of already significant climatic transition. Into this knowledge gap has emerged experimental results from the realm of global circulation models (GCMs).

1.2 TCs IN GCMs

Earlier generations of GCMs were generally not run at resolution sufficient to represent the physical structures of TCs, and thus such storms did not meaningfully appear in their outputs (Wehner et al. 2014). However, in recent years, models run at grid spacings approaching ∼25km have produced outputs containing TCs in numbers and/or intensities resembling those in best-track archives (Roberts et al. 2020).

Simulated TCs are counted and analyzed via tracking algorithms, which identify TC-like features in wind, pressure and other variable fields and capture their movements. Despite sharing basic physical underpinnings, model-generated storms and real life ones have major differences in morphology and intensity, which motivated the Pressure-based Hybrid Algorithm for Storm Tracking (PHAST), developed for this research (see Methods).

The advantages of direct TC tracking over extrapolation from environmental metrics, like Potential Intensity (PI) or Genesis Potential Index (GPI) (Bacmeister et al. 2014; Studholme et al. 2022; Emanuel and Nolan 2004), include that at such resolutions analysis can include detailed data about individual storm formations, trajectories and structural evolution. Certain metrics they can capture, such as storm lifetimes and landfalls, are not reflected in bulk-area variables at all. However, this specificity comes at the cost of statistical noise, with storm properties varying year to year even in stationary climates. Such randomness reduces the statistical significance of comparisons among climate scenarios, while at the same time the computational power required to resolve such storms limits the sizes of potential modeling data sets. Other work studying directly-modeled TCs under changing climates (Bhatia et al. (2018), Bacmeister et al. (2018)), have run their models as single-member ensembles, for time spans on the order of decades.

The results of direct tracking are comparable to statistical-dynamical downscaling, as implemented in algorithms like CHIPS and pepC (Emanuel et al. 2004; Jing et al. 2021). These seed potential storms superimposed over model outputs, which then grow or dissipate according to environmental variables, while being steered by prevailing winds. Such "synthetic" storms develop in intensity, travel along realistic tracks, and dissipate when they run out of heat energy or make landfall. With tuning of seeding and other parameters, downscaling outputs can match observed global storm numbers and intensities, and recreate TC trends in the historical record given corresponding forcings (Jones et al. 2017). However, the TCs that emerge from such methods do not in turn influence their broader environment, but rather exist only in post-processing. And with finer grids ($<\sim 1^\circ$), synthetic storm tracks and development

would be complicated by the presence of model-native TCs emerging in the same basins.

We see the promise of studying TCs in high resolution GCMs, even as compared to similar methods like localized model downscaling (Knutson et al. 2015), in its parsimonious relationship to native model dynamics. TC behavior in high-resolution runs is a function of overall model skill, dependent on what models predict about the specific weather systems necessary for TC formation and development. Direct tracking could be capable of incorporating the effects of unknown or poorly understood influences on TC behavior, including non-canonical cyclogenesis, and changes in TC formation areas with shifting global temperatures. Studholme et al. (2022) suggest that with changing latitudinal distributions of TCs under climate change scenarios, existing bulk-variable paradigms may significantly fail to account for changes in storm basin geometry and accompanying changes in cyclogenesis mechanisms. Approaches in which storms emerge directly from consistent underlying physics, rather than empirical formulations based on recent historical data, may then hold the key to understanding TC distribution patterns radically different than those of the present and near past.

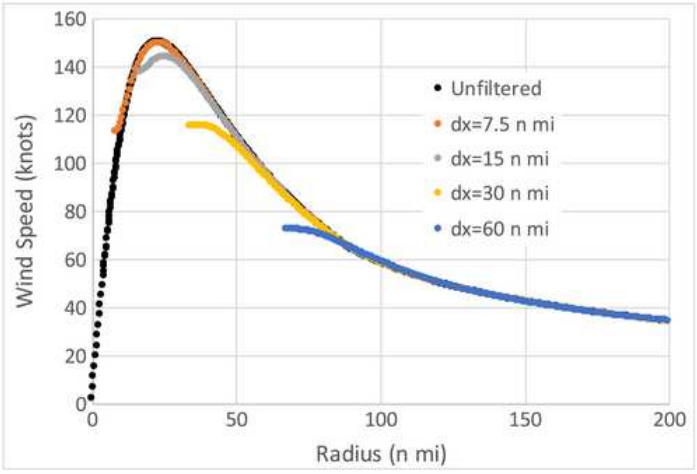

FIG. 1.1. Filtered radial (nautical miles) wind speeds (from Davis (2018)) for Hurricane Katrina as potentially represented by various grid spacings. Demonstrates intensity limitations of realistically rendered model TCs.

Consequences of this dependence of tracked storm behavior on small-scale model dynamics, however, include the possibility of systematic errors arising from model behaviors not yet well understood as we enter the high-resolution modeling era. But in turn, studying TC behavior in this new class of models has the potential to help elucidate model biases: Davis (2018) found that, given observed TC wind distributions and resolution limitations, strictly physically realistic ∼.25° GCMs cannot possibly produce realistic numbers of category 4 and 5 storms. Even given otherwise perfect model physics, maximum TC winds occur over such small horizontal areas, that averaging over such large cell areas will necessarily smooth out surface wind maxima considerably. Thus, GCMs at this resolution that do generate significant numbers of major storms, must suffer from biases leading to intensity exaggerations.

In this way, direct TC tracking, though dependent on the strength of existing model physics, in its limitations can recursively help inform future model development. However, this means direct tracking analysis (or indeed all study of non-tuned TCs in climate models generally), must be understood in tension as both reflecting the strengths and drawbacks of high resolution GCMs and their attendant emergent phenomena.

Davis further suggests that, based his analysis, evaluating modeled storm intensities based on wind speed is "not optimal." In light of this, we have developed a novel TC tracking algorithm with intensities based on central pressure, as described in Methods.

1.3 Climate Change and TCs

Under Kerry Emanuel's Potential Intensity theory, warming oceans can be expected to yield TCs of generally greater intensity, all else constant (Emanuel 1988; Walsh et al. 2016). However, within the context of chaotic weather/climate systems, it is difficult to extrapolate individual storm behavior from physical first principles alone, and a fair degree of uncertainty exists in regard to a warming climate's effects on TC number, intensity and other behavior.

Globally, Walsh et al. (2016) find in a review of studies of the recent/satellite era historical TC record, broad global trends toward TC distributions migrating poleward; reduced translation/track speeds; and increasing proportions of storms of category 4 and 5. Klotzbach et al. (2022) document a likely recent historical (1990-2021) decline in global TC frequency, along with rising numbers of category 4 and 5 storms, for a relatively more significant upward trend in such powerful storms' overall proportion.

These observations largely comport with findings, from a strong majority (Knutson et al. 2020) of GCM studies focused on future climate/emissions pathways: in a warming world, average TC intensity will increase, perhaps considerably. In a modeling study review, Knutson et al. (2020) find a mean +5% increase in maximum surface wind speeds given 2° of warming, and including only high-resolution model runs. This occurs alongside robust increases in the overall share of intense storms. Further, consistent with the exponential relationship of saturation humidity and temperature under the Clausius-Clapeyron relation, warmer TCs in a warmer climate are also found to yield mean 14% more precipitation under the same 2° assumptions. Less certain are other modeled, interconnected trends, toward reduced TC number; increasing absolute numbers of category 4 and 5 storms; and reductions in track speeds. Unlike in the Walsh et al. (2016) observational review, Knutson et al. (2020) do not find any robust trends in overall storm trajectories, in particular failing to find a global poleward shift in distribution.

Among the two papers helping form the basis our statistical/analysis methods, Bhatia et al. (2018), produced TC tracking results somewhat varying from the Knutson et al. (2020) review's lower-certainty reported findings. Using the Geophysical Fluid Dynamics Laboratory's HiFLOR model at .25° resolution, Bhatia et al. (2018) compare TCs in a baseline run representing 1986-2005, to two warming scenarios, 2016-2035 and 2081-2100 under RCP4.5. In each scenario, SSTs were nudged toward mean values for the 20-year period, and coupled atmosphere and land models run for 70 model years. Using direct tracking on HiFLOR's spontaneously arising TCs (including significant numbers of category 4 and 5), the authors find an overall increase in TC frequency in a warming climate. The 2081-2100 scenario is found to generate 9.1% more TCs each year than the baseline, arising from a mix of increased and decreased activity among different basins. This is accompanied by an increase in intense TC numbers and share as in other studies, with, notably, an 85% rise in category 5 storms in the same end of century scenario, and consistent increases in TC Rapid Intensification (RI) across all basins in both warming scenarios.

Knutson et al. (2020) find it challenging to reconcile models predicting a global decrease in TC frequency with a minority that show the opposite. They tentatively advance several potential explanatory mechanisms, but there is no consensus about how this decrease would arise given increasing intensity. Bhatia et al. (2018), however, argue that as their study directly modeled TCs for an unprecedented time span at high resolution, the HiFLOR results may have particularly strong predictive power in this domain.

Assuming early-stage TC genesis is broadly controlled by similar mechanisms to TC intensification, the widening geographic areas over which intensification will become likely (Bhatia et al. 2018) should, under the most parsimonious understanding of TC physics, produce increased frequency alongside increased intensity. Alternatively, in a physics of TCs whereby larger storms locally deplete the large-scale conditions necessary for formation (Emanuel 2022), a possible result of warming could be fewer storms, but more overall cyclone power as measured by total Accumulated Cyclone Energy (ACE), a greater Power Dissipation Index (PDI) (Emanuel 2007), and/or other energy-based intensity metrics.

In the face of some disagreement in GCM tempestologies, Sobel et al. (2021) write that only some climate-related TC changes predicted by models are understood by existing physical theory. Increased wind speeds and precipitation are found and supported by theory, observations, and model results; these and related findings comprise the most certain predictions we can make about TCs in a warming world. Other findings, such as a poleward shift in TC peak intensities, are supported by observations and some model results, but lack a robust theoretical explanation (Sobel et al. 2021). And finally, the

authors argue that TC frequency remains the most poorly bounded major question in understanding the relationship between TCs and climate, with little helpful, strong evidence from any direction of inquiry (Sobel et al. 2021).

The mechanisms controlling TC number remain poorly explained at even a basic physical level (Emanuel 2022; Walsh et al. 2015), with Sobel et al. (2021) writing of current global TC number, "We have little idea why the total number could not be even an order of magnitude greater or smaller." Observationally, it is broadly understood that TCs emerge in regions of warm sea surface temperatures (SSTs) and high vertical instability, and are limited by a lack of Coriolis vorticity at the equator itself. Cyclogenesis is further dependent on local vorticity and convergence conditions, and easily inhibited by vertical wind shear (Frank and Ritchie 2001). These factors have been incorporated into the indexes, like GPI (Emanuel and Nolan 2004) or TCG (Tippett et al. 2011), used to estimate TC occurrence operationally and in low resolution modeling. But these are basically relative measures, calibrated to historical observations, and they may not fully hold in climates which are radically different from present day.

In line with these observed large-scale controls, Walsh et al. (2015) do find a robust correlation in a suite of high-resolution models between TC formation and seasonal 500-hPa mean vertical velocity, consistent across models with different convection parameterization schemes and much stronger than for any other studied variables. A warming climate may result in a more stable tropical vertical atmospheric structure, making it more difficult to achieve the "deep convection" (Walsh et al. 2015) necessary to create TC seeds.

In this understanding, regardless of the overall mechanisms controlling TC formation and development with respect to climate, TC occurrence may be fundamentally limited by seeding, as opposed to, say, available energy or storm packing in time and space, alternatives discussed by Emanuel (2022) and also found by him to be relatively lacking. And if a vertical velocity effect/mechanism is in fact primarily responsible for reduced TC frequency in a warming climate, models that yield decreasing TC numbers are potentially doing so by depressing their rate of seeding, even as the storms that do form have access to more energy and more moisture to power their heat engines.

On shorter time scales, ENSO and other cycles affecting SSTs are known to substantially affect TC frequency in individual basins, with En Niño corresponding to substantial decreases in frequency in the Atlantic and Australia regions, and increases in some others (Sobel et al. 2021). Slightly different correlations may apply to other TC power/distribution measures.

Earlier warm periods of Earth's history, such as the Pliocene (5.3-2.6 mya), may have been characterized by significant changes in climate oscillations, including changes in ocean temperature gradients characterized as "permanent El Niño" (Callahan et al. 2021). This contrasts with a possible strengthening of the ENSO cycle that may occur at least transiently in a warming world (Cai et al. 2018; Callahan et al. 2021). Potential shifts in these oscillations create even more uncertainty in future TC forecasts, as periodicity stacked on top of mean variables change, confounds any attempt to draw inferences on TC behavior based on uncertain future climate.

With respect to TCs specifically, the paleotesmpestological proxy record, while potentially indicating periods of high and low local activity at proxy sites (Wallace and Dee 2022) in recent millennia, does not cover the Pliocene or other more distant analogues to contemporary climate change. Further, the piecemeal nature of TC proxy coverage, from record sources like sediment layering and tree rings, cannot fully capture basin-wide or global trends in a way comparable to GCMs or best track archives. It is thus especially difficult, in this domain, to independently check model results against what we know of the past.

Finally, independently of much of future TC behavior, global sea level rise threatens to worsen social and economic storm impacts upon landfall, significantly exacerbating storm surges in coastal communities (Sobel et al. 2021). This would be in conjunction with aforementioned increases in storm precipitation that will occur more or less directly as a result of greater atmospheric saturation humidity. Any potential additional climate hazards posed by mean TC power increases, track changes or other emergent basin and globe spanning phenomena, will then always be observed on top of those arising much more directly out of Earth system thermodynamics at a level much more fundamental.

1.4 Climate Intervention Technologies/Scenarios

Climate Intervention (or "Geoengineering" (Bellamy et al. 2012)) consists of proposed methods to mitigate the effects of climate change, apart from emissions reductions. Actions framed as Climate Intervention include land use changes/ecological modifications to increase carbon sequestration (Heck et al. 2016); direct chemical removal of CO_2; and various technologies intended to increase the Earth's effective albedo, Solar Radiation Management (SRM). SRM proposals include Marine Cloud Brightening (Mahfouz et al. 2023), space-based solar reflectors, and the method of Climate Intervention most commonly appraised in the research literature (Bellamy et al. 2012), Stratospheric Aerosol Injection (SAI).

As proposed, SAI would involve dispersal of sulfur dioxide (SO_2)/sulfuric acid aerosols into the stratosphere, several kilometers above the tropopause. To meaningfully reduce global temperatures, aerosol releases would represent tens of gigatons of SO_2 annually, deployed according to feedback algorithms intended to meet multiple independent temperature pattern, or other climatic goals (Zhang et al. 2022; Tilmes et al. 2020). This would likely be realized through the operation of a fleet of air tankers, carrying either SO_2 itself or S to react with atmospheric oxygen, at a cost of perhaps $2.25 billion per year in 2018 dollars (Smith and Wagner 2018).

The albedo effects and residence times of stratospheric SO_2 are such that SAI may represent the most technologically feasible and cost effective means of Climate Intervention available in the near future. It also has natural proxies in past volcanic eruptions that have lofted similar quantities of reflective aerosols into the high atmosphere (Benton et al. 2022), yielding periods of albedo-driven cooling, such as 1816's "year without a summer" (Schurer et al. 2019). As such, it has been the focus of significant ensemble modeling projects, including the GLENS and ARISE SAI ensemble projects (Tilmes et al. 2018; Richter et al. 2022).

These and similar SAI modeling research at the National Center for Atmospheric Research include simulations described in "Reaching 1.5 and 2.0°C global surface temperature targets using stratospheric aerosol geoengineering," (Tilmes et al. 2020). This paper presents results of a series of SAI modeling experiments conducted with CESM2, using the Whole Atmosphere Community Climate Model (WACCM6) configuration. The ensemble members are based on differing global emissions scenarios paired with more or less ambitious SAI temperature control goals. These emissions scenarios, based on CMIP6 scenario protocols, are run with and without SAI intervention to explore the climate and weather effects over the studied period for each run, 2020-2100.

WACCM6 as used here includes 70 atmospheric layers with a total height of 150 km (into the lower thermosphere), and extensive representation of atmospheric chemical dynamics (Tilmes et al. 2020). It is relatively well suited to rendering the chemical and thermodynamic effects of SAI in the deployments studied, including stratospheric wind patterns that govern aerosol migration and residence times.

GLENS and Tilmes et al. (2020), respectively, include experiments with high-emissions pathways (RCP 8.5/SSP5-8.5), with substantial sulfur quantities necessary to maintain temperature targets based on 2020 conditions, or temperatures 1.5/2.0° above pre-industrial conditions. This in contrast to much more modest interventions studied in ARISE. Such large-deployment scenarios are preferable for studying effects on high noise-to-signal phenomena like seasonal TC behavior, in which small effects

could be obscured by random variation. However, RCP 8.5-type scenarios may be unrealistic in light of recent progress in climate policy (Richter et al. 2022).

The SSP/RCP climate pathways used in Tilmes et al. (2020) are based on the findings of successive IPCC reports on consequences of climate change, assuming various future trajectories of GHG emissions (IPCC 2021). The terminal number in each pathway name denotes radiative forcing from pre-industrial conditions, in W/M^2. In this framework, SSP5-8.5 represents a high emissions pathway, at the upper end of what may be plausible by the end of the century. The experiment "GEO SSP5-8.5 1.5," in Tilmes et al. (2020), constitutes the forcings basis of our one of our experiments, with SSTs and other variable fields from this extreme intervention case acting on dynamic atmosphere and land models. With SAI deployment beginning in 2020, the SSP5-8.5 based scenario is modified toward achieving 3 temperature goals: global temperatures 1.5° above pre-industrial conditions (L0); maintaining present inter-hemispheric temperature gradients (L1); and maintaining present pole-to-equator temperature gradients (L2). This is achieved with the feedback control algorithm also utilized in GLENS and ARISE, with sulfur injections 5km above the tropopause, split among deployment locations at 15° and 30° north and south. Sulfur released at each latitude is adjusted based on temperature distributions achieved the previous year, with more or less at each to correct for prior imbalances. At this altitude, aerosols quickly diffuse to even distribution within their latitude bands, while more slowly migrating poleward through the Brewer-Dobson Circulation (Richter et al. 2022).

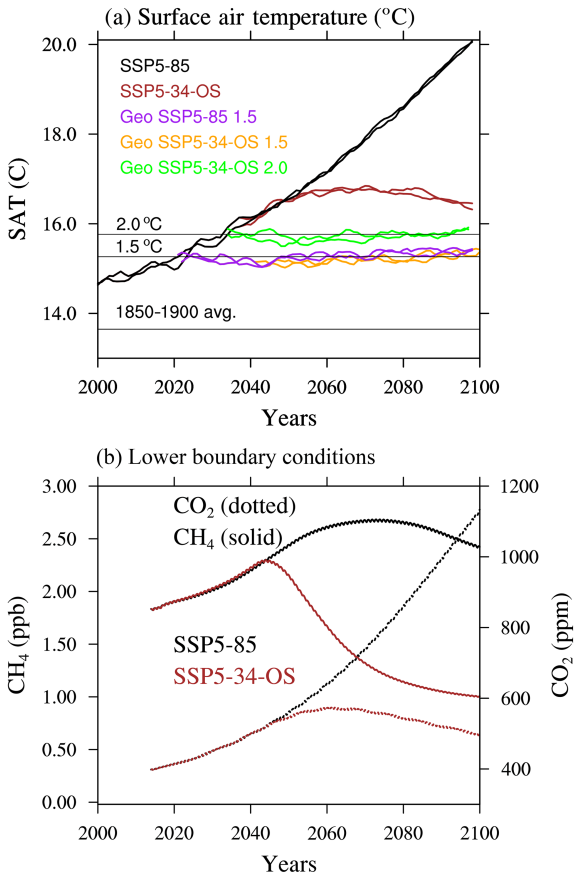

FIG. 1.2. Climate temperature and GHG trajectories, including Geo SSP5-8.5-1.5, corresponding to our SSP5-8.5-Intervention scenario, from Tilmes et al. (2020)

In Tilmes et al. (2020) Geo SSP5-8.5-1.5, scenario, SO_2 quantities released increase almost every year, especially at the 30° latitudes preferential for reducing warming's tendency toward polar amplification.

Total injection rates approach total 50 Tg/year by end of the century, with the assumption of continuous intervention through such time. The nature of potential SAI deployment is subject to manifold policy and physical uncertainties, including deployment in the face of unexpected climate tipping points (McKay et al. 2022), rogue single-state and non-state actors, and the masking of early SAI effects by regional and short-term variability, potentially leading to perceived failure (Keys et al. 2022).

Within this uncertain paradigm, the outcomes of any modeled climate intervention scenario serve mainly to outline potential action mechanisms and consequences of different technologies, rather than predict future climate conditions per se. As such, in the absence of large-scale intervention actually in progress, at best we can now analyze general tendencies and constraints of our possible climate futures; and this with the knowledge that the greatest unknowns remain, potentially, long-term climate policy and human decision-making itself.

1.5 Natural Analogues to SAI

SAI has drawn attention as a possible climate intervention due in large part to the effects of volcanic eruptions seen in the observational record, which similarly loft SO_2 into the stratosphere along with an array of other aerosols and gases. These events, notably including the 1991 eruption of Mt. Pinatubo, have caused measurable reductions in average global temperatures lasting several years (Aquila et al. 2021).

Significant disagreement remains as to the effects of volcanic eruptions on El Niño/La Niña (Khodri et al. 2017). Paleoclimate reconstructions and perturbation modeling indicate that ENSO response may depend on the latitude of volcanic events (Liu et al. 2018), but with large tropical eruptions more certainly tending to yield ENSO patterns that are more El Niño-like (Aquila et al. 2021; Liu et al. 2018).

Based on the heat engine understanding of TC formation and propagation, the most parsimonious relationship between volcanism/sulfur injection and TC activity is some sort of antagonistic effect. Given the dependence of TC genesis on SST thresholds hypothesized/observed to range from 25.5-27° C (Tory and Dare 2015), cooler oceans with smaller potential TC genesis areas should yield fewer storms of more equatorial latitude. However, to the extent TC number and power may not be limited by formation area or heat budgets (Emanuel 2022), other unexpected mechanisms could disrupt any simple SST-storm relationship that might otherwise be valid.

In the absence of strong paleoclimate data capable of connecting volcanic eruptions and TC statistics, Benton et al. (2022) conducted historical climate modeling based on the Last Millennium Ensemble

(LME) to study the TC pattern effects of sudden volcanism forcings against similar steady-state controls. Based on data produced via the CESM model, with forcings varied with volcanic and other signals reconstructed for the period, 1100-1850 CE was dynamically downscaled in WRF 3.9 to 30km grid spacing for selected 2-year periods following 42 aerosol-significant, mid-latitude eruptions. Downscaling was performed over a domain spanning the Atlantic and Eastern Pacific TC basins, strictly in the northern hemisphere. This data was compared to 150 years of downscaled simulation years with forcings held constant at 850 CE conditions absent volcanic and other energy budget-affecting climate variations. After application of the TSTORMS tracking algorithm (Zhao et al. 2009), TC statistics were compared between the control and volcanically active model years to discern whether the cooling and other modeled effects of volcanic aerosols had any measurable effects on storm occurrence and properties.

Benton et al. (2022) find that the overall effects of all modeled volcanic events on TC statistics not statistically significant for every calculated metric, including measures of intensity, number, lifetime and latitude. However, separating by hemisphere, NH volcanic events yield storms of measurably shorter lifetime, lower intensity and lower mean latitude than under control conditions. For PDI and ACE energy metrics specifically, combined and with respect to NH eruptions, the null hypothesis can be rejected at approximately the 2% level under the selected Anderson-Darling test. SH eruptions show somewhat smaller but opposite effects, with higher intensity, latitude and energy dissipation in the studied basins.

Looking at only the 5 strongest eruptions in each hemisphere, similar results are found, in which the strongest NH eruptions yield even shorter/lower TC average peak intensities, lifetimes and latitudes, while SH eruptions yield a smaller but opposite effect except with respect to power dissipation metrics.

The authors note several proposed mechanisms for aerosol-TC interactions in their introduction, including heat engine-type mechanisms in which lower SSTs or higher upper atmosphere aerosol layer temperatures reduce the efficiency of the TC Carnot cycle (Emanuel et al. 2013; Benton et al. 2022). However, another noted mechanism that may better explain differing hemispheric responses is proposed by Haywood et al. (2013), in which cooling caused by eruptions may alter global convection and precipitation patterns through shifts in the intertropical convergence zone (ITCZ).

Haywood et al. (2013), through observations and modeling, show that cooling in one hemisphere will tend to shift the ITCZ toward the opposite hemisphere by changing the behavior of the Hadley cell. They show that this phenomena, when driven by Northern Hemisphere volcanic eruptions, has contributed to drought events in the Sahel region in recent decades. This movement of the ITCZ changes patterns of convection and precipitation associated with the feature, and is also seen in further modeling

exploring the effects of hemisphere-asymmetric SAI injections (Haywood et al. 2013).

This sensitivity of low-latitude rainfall patterns to stratospheric aerosol distributions could also present a possible constraint/area of concern in considering SAI deployment. Avoiding significant shifts in the latitude of the ITCZ may thus be an important priority in constructing any SAI scheme (Lockley et al. 2022), and comprises an implicit goal of the GLENS/ARISE feedback algorithms, in the implementation of the interhemispheric temperature gradient (L1) constraint (Tilmes et al. 2020).

Benton et al. (2022) note observational studies of North Atlantic TCs following eruptions to suggest that this aerosol-ITCZ mechanism may extend robustly to TC activity. In modeling single-hemisphere SAI deployment, described as "analogous" to eruptions, Jones et al. (2017) hypothesize that shifts in the ITCZ southward away from the North Atlantic Main Development Region (MDR) will increase wind shear and impede TC formation, while a more northern ITCZ will promote such. Using climatological proxies, direct TC tracking (at 1.25° by 1.875° resolution), and statistical-dynamical downscaling, the authors study simulated North Atlantic TC frequency in RCP4.5, and scenarios representing both global and single-hemisphere SAI deployments. Obtaining somewhat contradictory results among the different approaches, Southern Hemisphere injections consistently yield greater North Atlantic basin activity than balanced or Northern Hemisphere alternatives; and based on direct storm tracking and index correlations, may - in spite of heat-engine effects - produce significantly more North Atlantic storms than even non-intervention RCP 4.5.

The authors demonstrate the salience of an ITCZ-mediated mechanism through correlation of TC numbers/proxies with North Atlantic MDR wind shear, SST anomalies and total precipitation. Moving the ITCZ away from the Northern Hemisphere will tend to increase shear while reducing SSTs and precipitation (and vice versa), all results that are found to occur in the model with Southern Hemisphere SAI and to correspond to reduced TC activity.

These mechanisms should remain important regardless of the causes of any hemispherically differential cooling (Jones et al. 2017), and apply to both volcanic eruptions and any albedo-based means of climate intervention.

The Earth's current TC development regions are shaped by continental geography and associated SST patterns, and each basin likely has its own unique relationship with ITCZ effects. However, as significantly more storms occur in the NH basins than in the SH basins, to first order, enhanced NH cyclogenesis paired with depressed SH storm formation, may be likely to yield greater overall frequency. Further causation-focused research, however, may be needed to determine the extent of ITCZ-TC

relationships in other basins.

While TC formation/frequency constraints remain poorly understood, we can begin to try to predict storm responses to SAI based on observed responses to current global warming and past episodes of volcanic cooling. These can be supplemented by effects and relationships found in model scenarios. Based on the existing literature, we can outline 5 varyingly well-described potential mechanisms affecting TC distribution under warming scenarios as mitigated by SAI. These include: (1) overall global SST reductions, via heat engine effects; (2) amelioration of polar amplification, with any concurrent shifts in basin area; (3) the emergence or prevention of changes in mean ENSO index; (4) shifts in the ITCZ driven by hemispheric temperature asymmetries; and (5) relative increases in TC seeding rates brought about by halting shifts toward greater atmospheric vertical stability. In the Results and Discussion sections of this paper, we will attempt to link any model-observed changes in TC statistics to one or more of these theorized mechanisms. These will provide a framework for understanding how SAI, relative to unmodified warming, may shift regional and global patterns of storm occurrence; and allow us to assess the certainty level of storm activity forecasts obtained from our models.

Through this process of comparing scenario results and drawing causal connections, we can begin to help illuminate the relative degrees of local and global TC hazards arising from both climate change, and intervention to ameliorate it. At different scales, SAI could bring storm patterns back into line with those in a pre-warming/historical climate, or could push global and regional tempestologies in directions largely without precedent. By identifying which control mechanisms may dominate storm development and evolution under SAI, we can create outlines of potential TC hazard profiles with salience extending well beyond the results of these specific runs.

CHAPTER 2

METHODS

2.1 MODEL CONFIGURATION

Our experiments are run within the EarthWorks model currently under development in collaboration between Colorado State University, the National Center for Atmospheric Research (NCAR), and other research institutions. Intended to bridge modeling of climate and weather phenomena at radically different scales, project goals include runs at a <4km horizontal grid spacing. At this and similar grid spacings, EarthWorks will serve as a Global Storm-Resolving Model (GSRM), capable of representing global climate behaviors while also capturing small scale phenomena resulting from and contributing to climate processes. In this way, problems at the intersection of climate and weather, including TC responses to climate change, can be addressed comprehensively across scales and domains.

EarthWorks is built on a foundation provided by the Community Earth System Model (CESM), an open source model maintained by the atmospheric science research community and utilized in a range of global and large-scale experiments. CESM includes components representing physics and chemistry of the oceans, land surface, and atmosphere. However, having been developed for large-scale simulations at relatively lower resolution, CESM is reliant on parameterizations to represent phenomena that at storm-resolving resolution should be directly simulated.

With parameterization, small-scale atmospheric phenomena like turbulence, and surface fluxes including evaporation, vegetation cover, sea spray, etc, are represented with simple formulaic assumptions for each grid cell. However, as model resolutions grow finer, phenomena that were once best represented through parameterization may eventually be directly simulated. Among the goals of the EarthWorks project, is to address new biases and errors as CESM physics is brought to GSRM scope.

Another notable feature of EarthWorks with respect to TC modeling is its use of the MPAS dynamical cores, based on hexagonal Voronoi meshes for atmospheric, ocean and ice components (MPAS-A, MPAS-O, MPAS-I) (Randall et al. 2019). Understanding of the performance of hexagonal grids at high resolution is limited, but they potentially hold important advantages in representing TCs.

Our experiments in this paper are conducted using ∼30km diameter grid spacing, with 58 vertical levels up to 40km height. GCMs with this horizontal spacing can be understood as representing the edge of the GSRM resolution range. Based on prior model outputs, this is fine enough to yield realistic numbers of TCs with a realistic distribution of central pressures, and is comparable to earlier global

TC modeling studies conducted at ∼.25° resolution with other grid geometries (Bhatia et al. 2018; Bacmeister et al. 2018; Irvine et al. 2019). With our present model configuration, running simulations at ∼30km spacing also creates computational costs of approximately 100,000 CPU core hours per model year, while generating potentially tremendous volumes of data. Given current computing availability, longer climate simulations cannot really presently be conducted at spacings any finer, and so for the foreseeable future, this scale is about where TC GSRM research must remain.

2.2 SAI/Forcings

Forcings for our experiments are based on outputs from the WACCM model described in "Reaching 1.5 and 2.0°C global surface temperature targets using stratospheric aerosol geoengineering," (Tilmes et al. 2020) as discussed in Introduction. While maintaining EarthWorks' dynamical simulation properties otherwise, data from WACCM ensemble members is used to force SSTs, sea ice cover, and SO_2 sources, with GHG concentrations taken from corresponding EarthWorks historical/SSP scenario presets. SST and sea ice are forced on a daily basis, while SO_2 production (rendered in 3 dimensions) is forced monthly. All three variable fields must be interpolated onto the EarthWorks hexagonal grid. These forcings create atmospheric conditions in line with Tilmes et al. (2020)'s studied climatologies, with SSTs themselves directly comprising an important element of TC formation conditions.

Forcing SSTs carries the drawback of not representing storm-induced turbulent mixed layer deepening (Bacmeister et al. 2018). As such, unlike in the physical world, TCs will not leave a path of cooler SSTs in their wake, and this may potentially remove a negative feedback on overall TC formation rates. However, if TC number may be fundamentally limited by seeding (Emanuel 2022) rather than available energy, and TC cold wakes make up a very small fraction of storm basin area at any given time, this lack of a mixing effect is likely negligible in determining storm frequency.

By contrast, the self-limiting effect of storm-driven ocean cooling means that models with fixed SSTs may actually be missing an important factor limiting storm intensity. However, given the range of storm intensities (Wehner et al. 2014; Irvine et al. 2019) reported in GSRMs with and without fixed ocean temperatures, and inherent limitations of representing storm intensity at resolutions like ours (Davis 2018), this effect is likely second-order.

With our forcings from Tilmes et al. (2020) and related NCAR-conducted experiments in CESM2-WACCM, we have constructed three climate scenarios intended to establish baselines for TC behavior in EarthWorks, and study the tempestological effects of both severe global warming and potential SAI

responses. These are:

- **Control Run**, with forcings based on the years 1990-1999 (Danabasoglu 2019a) (ensemble member r1i1p1f1) in CMIP6. This is well within the era of satellite TC observations, but likely before most appreciable change in climatic TC influences.
- **SSP5-8.5**, with forcings based on the years 2090-2099 in CMIP6 ScenarioMIP SSP5-8.5 (Danabasoglu 2019b) (ensemble member r1i1p1f1). Extremely strong warming signal that should make clear any significant TC-climate relationships of significance.
- **SSP5-8.5-Intervention**, with forcings data for the years 2090-2099 from Tilmes et al. (2020) scenario "Geo SSP5-8.5 1.5" (ensemble member 001). Based on SSP5-8.5 trajectory, but with SAI deployment beginning in 2020 sufficient to keep global mean temperatures at 1.5° above pre-industrial conditions as well as meet secondary climate goals.*

The first part of our Analysis consists of comparing TC tracking results from our Control Run against best-track data for the same time period from IBTrACS (Knapp et al. 2023). To the extent our combined model/tracking algorithm system is able to faithfully reproduce the observed contours of global tempestology as they existed in the 1990s, it will build confidence in our experimental results.

Our two future scenarios will allow us to interpret differences in TC properties in light of significant changes to related climate variables. We will seek to examine changes in ENSO and the distribution of storm-generating SSTs, among other possible mechanisms, to determine if SAI has the potential to significantly reduce/alter TC risks. As well, our SSP5-8.5-Intervention scenario constitutes among the first attempts to directly model tropical storms in high resolution under climate intervention (Irvine et al. 2019), and the first to so utilizing a realistic SAI regime.

2.3 PHAST Tracking Algorithm

As discussed in the Introduction, TC-like features appearing in the outputs of models at lower-end storm-generating resolutions either do not, or should not (Davis 2018) generate winds with a full range of realistic intensities. Based on model native wind speed, storms tracked in our Control Run scenarios very rarely achieve CAT 3, and never attain intensities any greater.

Seeking alternative means of diagnosing the intensity of model storms as they would manifest in the physical world, we turned to the literature quantifying empirical relationships between TC category/wind wind speed and other variables. The literature on constructing Wind Pressure Relationships

*Includes 5 days of interpolated SST data, September 26-30 2097, as patch to data error.

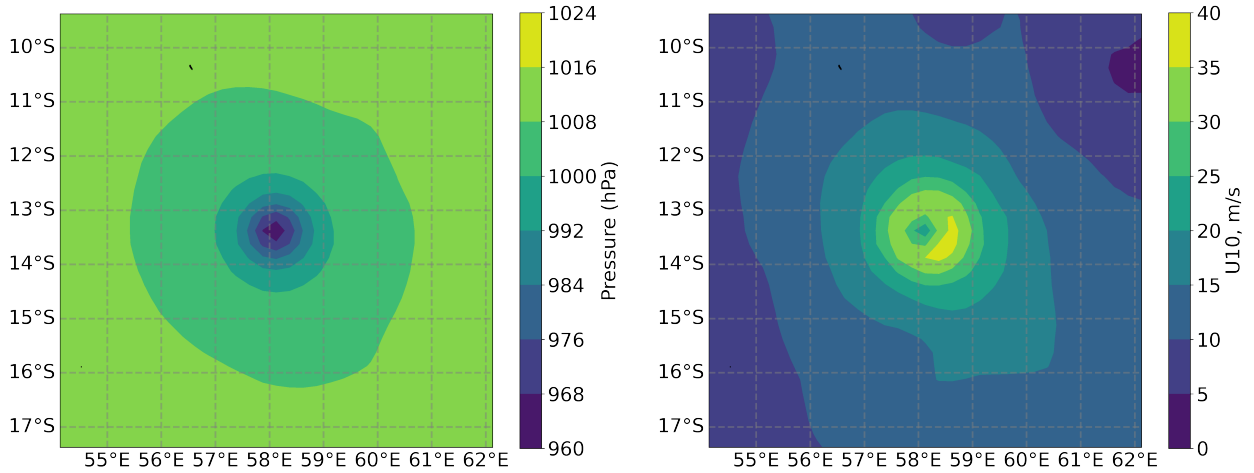

FIG. 2.1. Contour plots of pressure and wind fields for a South Indian basin storm, Control Run.

(WPRs) demonstrates tight correlations between TC central pressure/pressure deficit and max observed wind speed (Knaff and Zehr 2007, figure 5). This allows minimum central pressure, which is often easier to observe than maximum winds, to serve as a stand-in for such and for overall storm intensity.

Similarly, in EarthWorks model outputs, minimum and near-minimum pressures occur over a much larger area within each storm eye than wind maxima outside of such, creating a more robustly measurable feature. As well, TC central pressures in EarthWorks outputs map more closely to real-world distributions, with pressure minima arising equivalent to even strong CAT 5 storms.

In light of this contrast in the model properties of these possible intensity measures, we decided to update an existing tracking algorithm, TSTORMS (Vitart et al. 1997; Zhao et al. 2009), to take advantage of mapping pressure data onto wind-based storm categories through interpretation of pressure minima via a WPR relation.

As part of our modifications to TSTORMS, after candidate vortex features at each time step are stitched together into candidate TC tracks, storm intensity minimum requirements are applied based a mix of native wind and pressure constraints. Rather than requiring a minimum 17 m/s V_{max} across three model days, PHAST utilizes a dual requirement of native winds of 10 m/s, and central pressures corresponding to 17 m/s in our chosen WPR (see Appendix) across the same span(s). After this initial intensity filtering, measured intensity is then based entire on mapping PSL onto calculated wind speeds and resulting Saffir-Simpson categories.

Other adjustments to TSTORMS include changes in variable window sizes and requirements for maxima/minima identification based on the possibility of storms occurring closer together in space

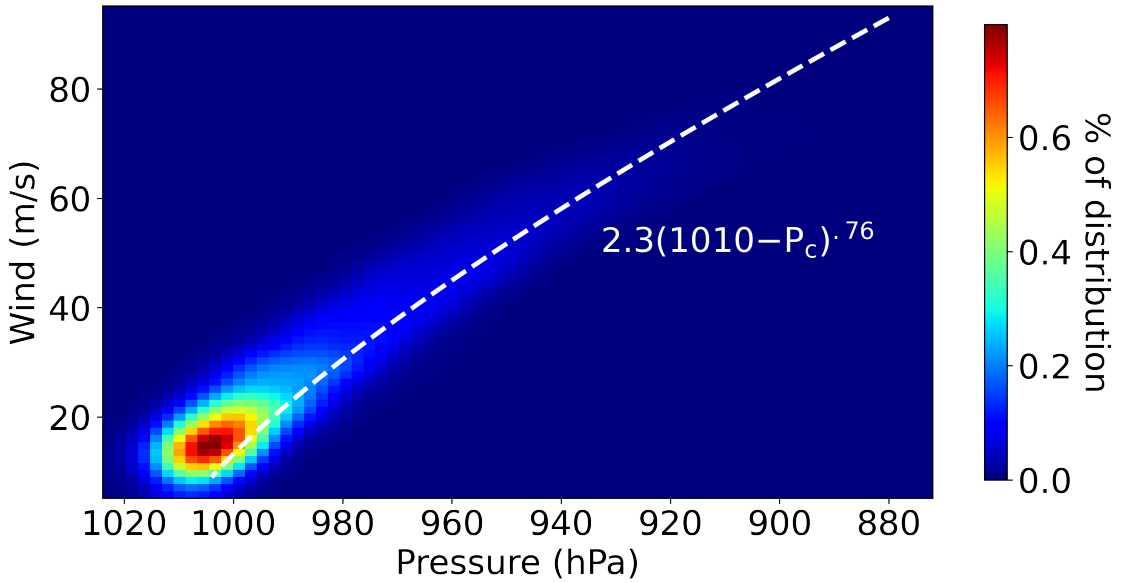

FIG. 2.2. Two-dimensional histogram of USA_PRES, USA_WIND (1-minute wind) variables for IBTrACS TC (TD/TS+) data 1980-2022, superimposed with the PHAST WPR. Smoothed with Gaussian filter $\sigma = 2$.

than the 6° in latitude/longitude allowed previously. A number of TCs in EarthWorks output at our ~30 km resolution have passed close enough to each other for TSTORMS tracking to start to treat them as a single storm despite maintaining distinct geometries, creating phantom storm deaths/births and leaving us unable to meaningfully track some storms experiencing the Fujiwhara effect (Fujiwhara 1921). Thus, among other adjustments in PHAST, candidate vortexes need only represent the highest absolute vorticity in a 2° box about themselves, creating more maxima detections, but seemingly reducing overall TC detection error.

Finally, as in other configurations of model outputs and storm trackers (Han and Ullrich 2024), PHAST initially misidentified subtropical systems, particularly off the coast of South America and in the Mediterranean, as TCs. Broadly, TC genesis is extremely rare outside the world's main tropical cyclone basins, and detected storms in these other areas are in fact subtropical systems with important differences from TCs in structure and smaller ranges of intensity.

To quickly distinguish TCs from other convective systems, we impose a storm-center SST requirement to ensure that storms are occurring in conditions consistent with tropical storm climatology. To be identified as a valid TC in PHAST, a candidate convective system's pressure-center track is matched with SST outputs for the same grid positions in time and space. Each point on the track is tested for whether it represents a storm-SST conjunction with surface temperatures of at least 27° C, not on/over

land. Valid TCs meet these conditions for at least one time step over their lifetime.

This temperature threshold comes from the literature on thermodynamic bounds on cyclogenesis (Tory and Dare 2015). It represents a highly conservative lower bound on TC formation temperatures, which effectively removes virtually all false positives in our storm track data. A few valid model TCs may be disqualified under this filtering, but track numbers in the world's main TC basins appear virtually unchanged, and the main group of false negatives arising here likely represent low intensity TS/TD storms that do not factor into our main analysis.

2.4 Best Track Data/Method Calibration

TC metrics for our future experimental cases are measured against results for our Control Run, which must itself be evaluated against TC observations from the historical record. For this purpose, we use the all-basins tropical storm track data from the IBTrACS database (Knapp et al. 2023, 2010), a global compendium of satellite and in-situ observations/interpretations. The database does not represent a fully comprehensive record for all basins at all times, but is likely largely complete for sufficiently intense storms in the global satellite coverage era. On this basis,

ERA5 re-analysis data (Hersbach et al. 2020) was considered for our Control Run calibration. But due to systematic errors in the properties of TCs that occur within it (Hodges et al. 2017), and the inherent resolution-based limitations it faces representing TC intensity (Davis 2018), we ultimately decided to limit our comparisons to our own model results and to best-track data.

To further increase the reliability/salience of our comparison methodology, unless otherwise noted, all analysis of TC tracks between both model and best-track data is limited to storms CAT 1+ (IBTrACS categories taken from "USA_SSHS" variable). This likely increases the reliability of both best-track data for the studied period, and limits the rate of false positives in PHAST. This choice has the downside of reducing our effective sample sizes and statistical significance. As well, ignoring TS/TD systems may have the effect of excluding some outputs representing emergent non-canonical cyclogenesis mechanisms in a changing climate, particularly weak storms occurring further poleward than is typical (Studholme et al. 2022). But if overall cyclogenesis favorability in a time and place has some relationship with overall storm intensities, these signals should still appear in strictly CAT1+ data as well. And overall, we feel that a focus on hurricane strength TC-intensity storms allows us to exclude enough observational and methodological artifacts to justify this reduction in scope.

CHAPTER 3

CONTROL RUN VS. IBTRACS COMPARISON

3.1 STORM NUMBERS AND INTENSITIES

Initial track analysis of our Control Run shows high fidelity for historical TC behavior. Using forcings for the 1990-1999 period, similar numbers of tracked storms are generated and detected as compared to IBTrACS (605 vs 517, respectively). Storms occur across a range of intensities mirroring real-world distributions, albeit with significantly fewer major storms (CAT3+) (figure 3.3). This could be a result of resolution effects, with highly localized convection extrema necessary to resolve to create realistic TC central pressures. Alternatively, some other artifact of our model physics, such as its parameterization of turbulence (Nardi et al. 2022) or some other small-scale process, may be creating systemic errors especially apparent in the TC context.

Nevertheless, we may understand the intensities of storms in our Control Run as mapping onto real-life TC intensities, and likely constrained/influenced by a host of similar climatological factors. Storm seasonality matches well with real-life basin behavior (see figure 4.9) (NOAA 2024c), seemingly driven by similar temporal variation in TC favorability. Mean decadal global surface temperature in our Control Run (with forced SSTs, dynamic land temperatures) is 15.3° C, well in line with observed temperatures over the same period, and apart from some seeding events involving land-based weather systems, differences in salient climatic conditions should be minimal.

Insofar as EarthWorks is in fact capturing fundamental cyclogenesis and intensification processes, we can interpret any significant changes in this distribution in our experimental runs as potentially reflecting fundamental shifts in overall global tempestology.

The lowest TC central pressure recorded in our 1990s Control Run, 899.2 hPa, corresponds to a WPR wind speed of 82.3 m/s (296 km/h). This is toward the upper end of observed TC intensities, and demonstrates that our model and method can yield a full spectrum of such intensities, if not a balanced distribution. This indicates that our downward intensity biases are either not fully consistent across model time and space, or are partially balanced by occasional variable biases in the other direction. Understanding the nature and extent of potential issues in TC representation is complicated by the multitude of local processes we must simplify/parameterize to construct GCMs, and the unpredictable biases these may introduce in a highly emergent system.

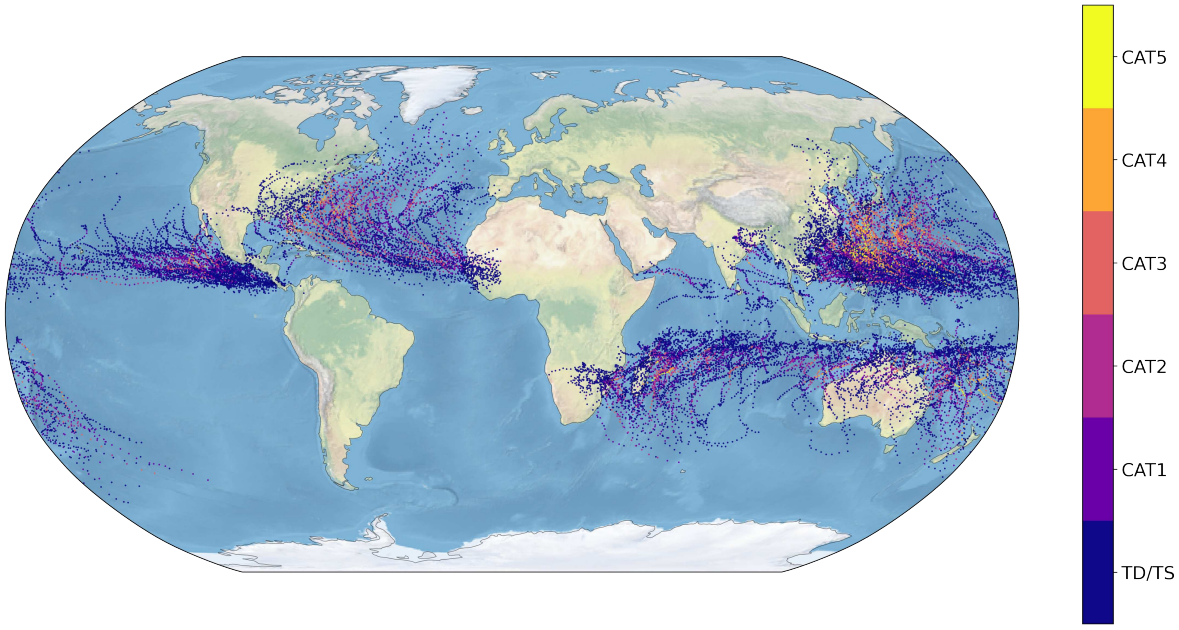

FIG. 3.1. PHAST-generated TC tracks produced from Control Run data covering 1990-1999. Excludes systems that never achieve CAT1+ intensity based on PHAST WPR.

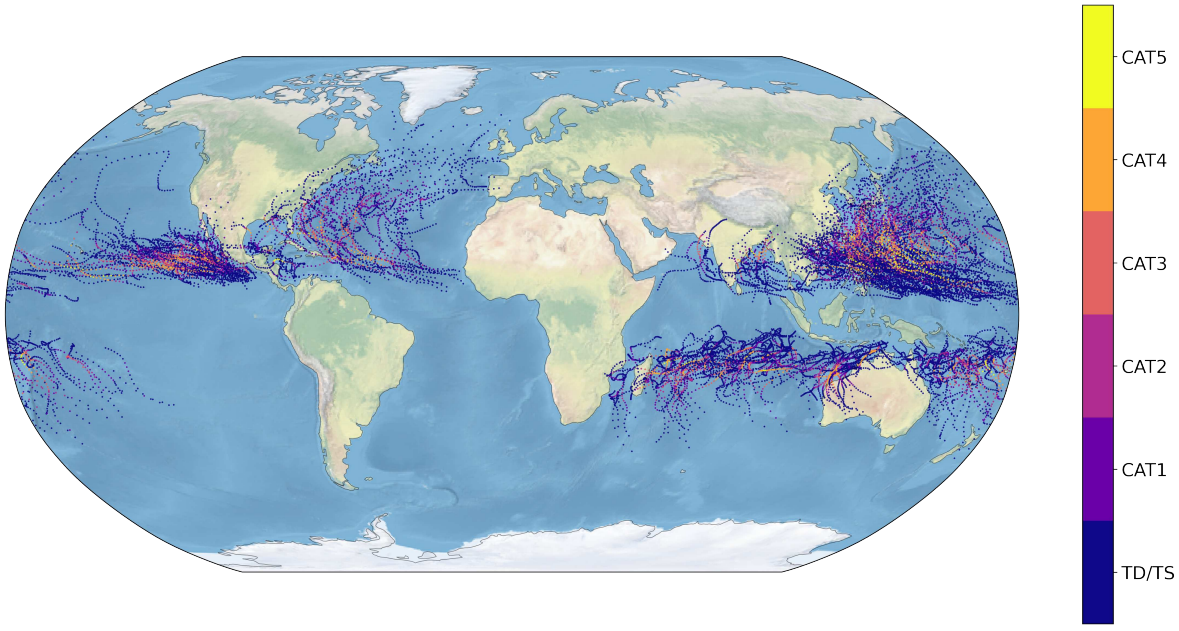

FIG. 3.2. IBTrACS global best-track TC data covering 1990-1999. Excludes systems that never achieve CAT1+ intensity, based on given IBTrACS category labels. Reduced to 6-hourly track frequency.

3.2 BASIN AND LATITUDE DISTRIBUTION

Using basin geometries from Bhatia et al. (2018), and dividing both IBTrACS and EarthWorks track data by storm origin, we find fairly similar distributions of TCs among the world's basins (compare

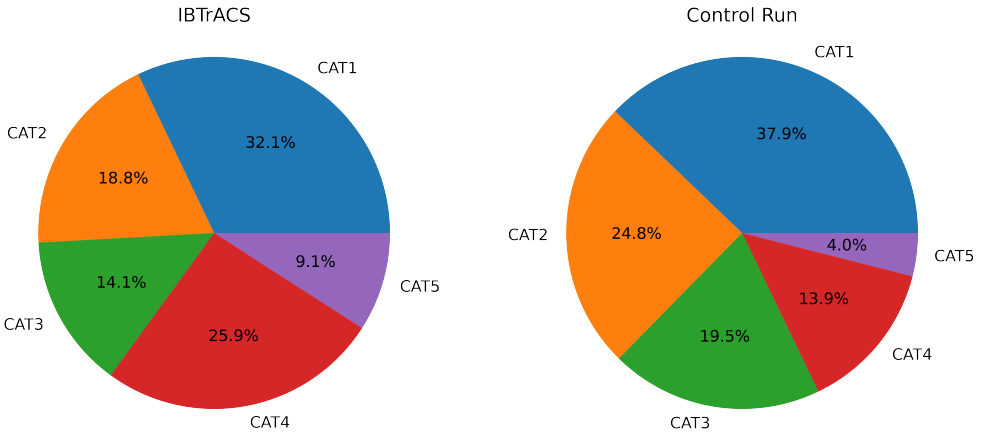

FIG. 3.3. Category Distributions (max lifetime intensity)

figures 3.1, 3.2, see figure 3.4). Some IBTrACS categories data may be affected by observational data rounding (Nayak et al. 2024), although applying the same rounding to EarthWorks data shows this affect is likely minimal overall. Broadly, our Control Run has a somewhat lower share of storms occurring in the Pacific. But overall, the basin geometry of storm trackways, origins and directions of movement are represented with great affinity. TCs occur with great density at their cyclogenesis region in the East Pacific, and along much of their range in the West Pacific.

Major differences in basin geometry between these data sets occur as a function of detection lifetime; the lengths of time TCs are tracked very early in cyclogenesis, and following extratropical transition. This contributes to a significantly poleward tail of EarthWorks SH storm distribution, with feature tracking extending somewhat further down than in IBTrACS, and a mean SH storm latitude of 18.2°, vs. 16.1° for IBTrACS. Otherwise, the overall global mean storm latitude remains similar (7.8° vs. 8.8°), as do NH means (19.5° vs. 18.6°). Lifetime effects are perhaps most clearly visible at the start of the North Atlantic trackway, with pre-TC features in EarthWorks forming the start of storm tracks over West Africa, well before/east of where they do so in IBTrACS.

Although tracked storms in our Control Run cover sometimes much longer distances than their best-track counterparts, their lifetimes are similar. EarthWorks storms that achieve CAT1 at any point, are alive for a mean of 11.2 days, while the mean CAT1+ IBTrACS storm occurs over 3-hour steps comprising 11.0 days. In contrast, such EarthWorks storms achieve a mean translational velocity, based on 6-hour

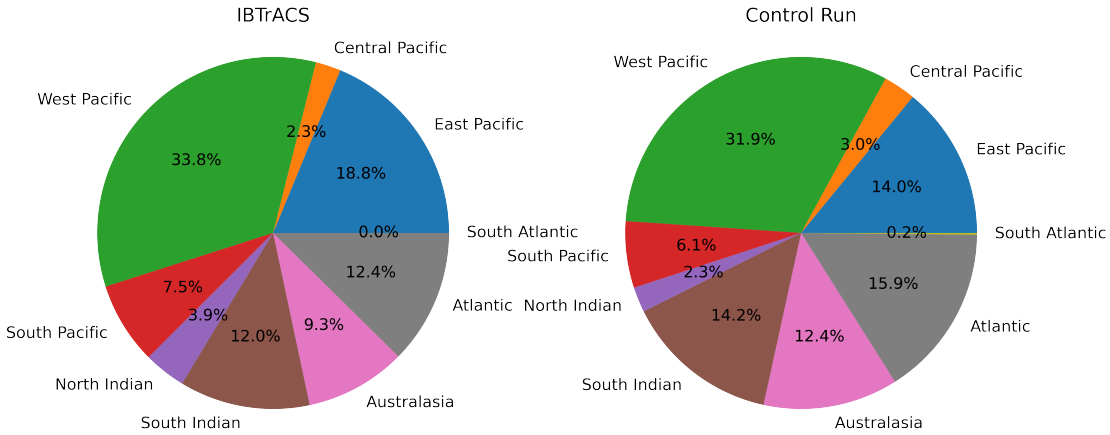

FIG. 3.4. Basin Distributions (system origin)

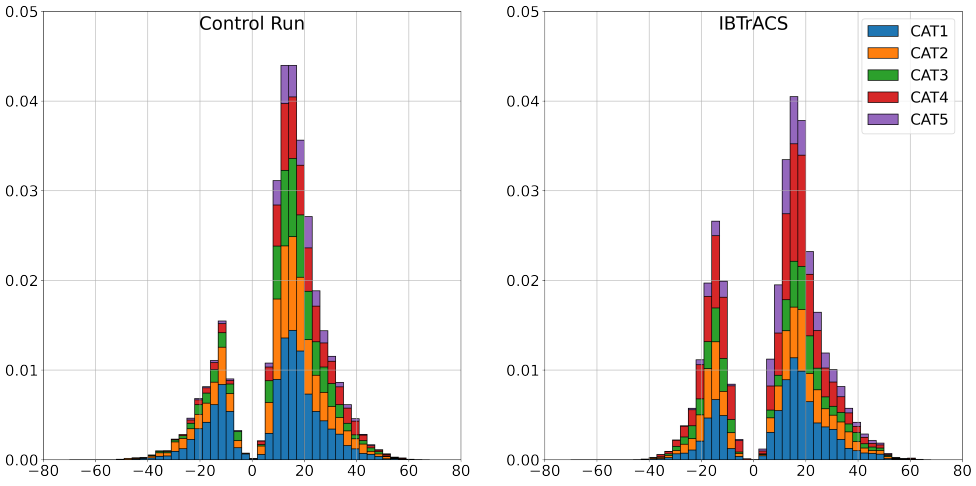

FIG. 3.5. Latitude occurrence distribution by storm category (max lifetime intensity); 6-hourly track data for EarthWorks, 3-hourly for IBTrACS.

time steps, of 20.5 km/h, while every two 3-hour steps, equivalent IBTrACS features on mean have travelled at 17.5 km/h. Given that our EarthWorks/PHAST tracks appear to include earlier and/or later stages of storm evolution (figures 3.1, 3.2), these higher velocities and longer tracks with equivalent lifetimes indicate a faster TC life cycle; altogether, EarthWorks storms form, move along their trackways and then dissipate consistently faster that in reality. Only some of the translational speed difference

seen here is due to intensity-related effects, as our EarthWorks and IBTrACS translational velocities while storms are actively CAT1+ are, respectively, 20.0 km/h and 17.7 km/h. Rather, storm translation occurs faster in our simulation across development stages, leading TCs to progress through their evolution from tropical disturbance to post-tropical storm more quickly as well. This may also have the effect of reducing peak storm intensities, as systems spend less time over patches of ideal SSTs.

3.3 Storm Properties

Storms seen in EarthWorks, like those in other GCM's (Nardi et al. 2022) can be broadly described as "donuts."* That is, in magnitude 10 meter wind (U10), outgoing longwave radiation and other variable fields, fundamental convection processes will create an eye geometry broadly corresponding to that expected from fundamental storm physics (see figure 3.6). Central pressure and eye wall wind speeds vary inversely on curves similar to those derived from observations. But partly due to resolution limitations, and partly due to biases in model dynamics/parameterization (Nardi et al. 2022), finer scale features seen in the real world may not be apparent. Thus, GCM-generated TCs, even when yielding accurate population-level features, bear important differences on a storm-level basis with observations.

Given the largely correct basin distribution patterns and macro behavior exhibited by EarthWorks, CAM, HiFLOR, etc (Bacmeister et al. 2018; Bhatia et al. 2018), it is likely that most of the fundamental controls on TC distribution can be found at scales $\sim .25°$ and above. We therefore feel confident in analysis of overall GCM storm trends at this resolution relating to such, if perhaps less so with respect to precipitation and other properties more closely tied to exact storm geometry.

Bhatia et al. (2018) discuss observations of storms undergoing rapid intensification (RI) in HiFLOR, and compare rates of such to those seen in IBTrACS and ADT-HURSAT databases. Similarly defining RI as storm intensity change of +30kts (15.43 m/s) in 24 hours, we find that using the PHAST pressure-intensity relation to evaluate storm evolution, 92.9% of CAT1+ Control Run storms undergo RI over their lifetimes, including 96.5% of major storms that do so. Expanding in this instance to include sub-CAT1 storms, we still find an overwhelming majority, 80.2% (795/991) experiencing RI.

These findings are similar to those for major ADT-HURSAT storms as analyzed by Bhatia et al. (2018), and reflect reality insofar as most intense TCs are observed to experience RI. But as compared to the IBTrACS and HiFLOR data sets, and compared to RI lifetime shares for all three Bhatia et al. (2018) historical period data sets, significantly overstate the speed at which most storms generally intensify.

However, such figures may partly reflect the geometry of our WPR curve. Using an alternative NHC

*Personal correspondence with Colin Zarzycki and others.

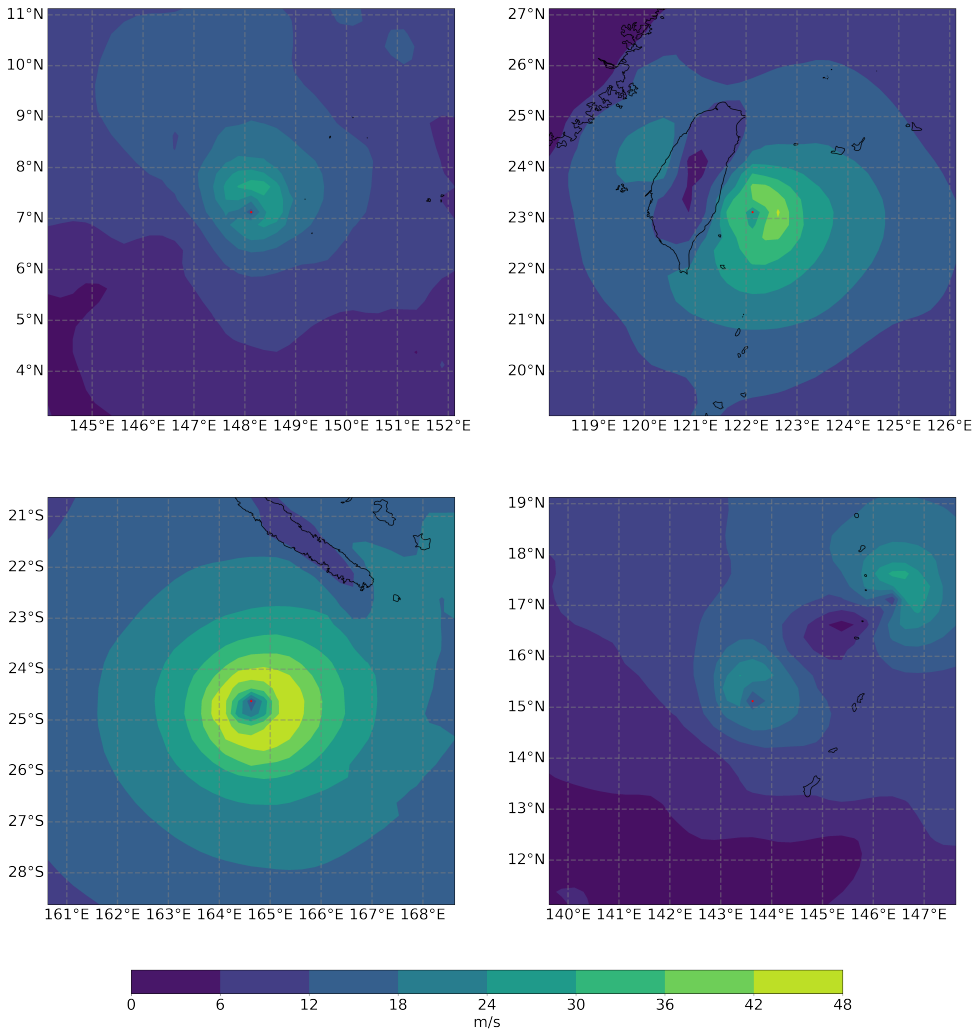

FIG. 3.6. Model-native U10 contour plots for selected TCs, Control Run. Clockwise from top left: West Pacific storm with PHAST-calculated TS intensity; CAT3 storm making landfall on Taiwan; TS experiencing Fujiwhara effect rotation relative to another system; CAT5 TC south of New Caledonia.

definition of RI as a drop in minimum pressure of 42 hPa over 24 hours (Holliday and Thompson 1979), we find that all Control Run TS/TC storms, CAT1+ TCs, and major storms, respectively, experience RI 15.4%, 25.3%, and 50.4% of the time. The all-Control Run storms see a boost in mean max WPR intensity from 39.0 m/s to 56.5 m/s, with RI vs. without, and in median max intensity from 36.6 m/s to 56.8 m/s. The magnitude of this effect however is still much smaller than those seen by Bhatia et al. (2018) (figure 4) both in best-track data sets and in their HiFLOR experiments.

These pressure-based RI figures are in line with the overall lower frequency of major storms, and lower intensity of such, in our EarthWorks-PHAST outputs as compared to best-track data. And we do see a significant correlation between RI and lifetime maximum intensity here, albeit not to the same extent as observed in the physical world. These exploratory RI findings for our Control Run data set potentially points to the overall preferability of pressure-based metrics for evaluating TCs at this and similar model resolutions. Overall, rapid intensification may not be driving storm development as much in EarthWorks as it does in observations or in Bhatia et al. (2018)'s model native-wind evaluations. And taking into account our limited model-TC sample sizes here, may not serve here as an effective analysis paradigm with respect to TC behavior.

CHAPTER 4

WARMING, WITH AND WITHOUT INTERVENTION

4.1 STORM NUMBERS AND INTENSITIES

In line with the bulk of prior modeling/earlier literature, severe warming in EarthWorks yields a world with fewer TCs, but a greater number of CAT5 and outlier/extreme intensity storms. The highest PHAST WPR wind speed observed in SSP5-8.5 is 97.5 m/s, and the scenario includes 8 storms tracks with speeds above the Control Run max, 82.3 m/s. Taking the integral of storm occurrence days over intensity for fig 4.5, the SSP5-8.5 scenario includes 64.25 days of combined CAT5 storm existence, vs. 39.25 in our Control Run, and with 34 storms achieving such over a decade vs. 24. Increasing in number, maximum intensity, and time spent in CAT5 intensity range, the most powerful storms in this warming scenario could represent a significant, disproportionate increase in natural disaster risk, on account of the exponential relationship observed between storm intensity and damage (NOAA 2024b). This would be countered in part or in full by an overall reduction in both total storm number, and even specifically in major storms (CAT3+) overall.

Notably, though both future scenarios do represent significant shifts in climate from historical conditions, global TC counts only change substantially with warming that's unmodified (461 in the SSP5-8.5 run, vs. 606 in SSP5-8.5-Intervention). SAI returns global storm number roughly to current observed levels, in spite of important climatological differences between SAI-cooled climates and same-temperature unmodified ones (Tilmes et al. 2020).

The most parsimonious explanation of global trends toward increased storm intensity and reduced storm number with warming, is a combination of higher vertical stability and/or vertical shear inhibiting cyclogenesis, combined with higher SSTs fueling more powerful heat engines. Comparing the scenarios' intensity curves, however (figure 4.2), while our Intervention experiment roughly matches up with our Control Run distribution, the occurrence of CAT5 and stronger CAT4 storms more closely resembles the magnification seen in SSP5-8.5.

Our Intervention scenario, then, does not represent a linear part-way state between our warming and historical runs in terms of intensity distribution, but rather includes elements of both. Possible explanations for this apparent linear independence include basin-scale effects, physical non-linearity in stability or heat engine mechanisms, or changes in global SST patterns not present in either unmodified scenario. Given that introduced SO_2 in our model should largely precipitate out of the stratosphere over

the poles via the Brewer-Dobson circulation, and comprise a fairly small share of overall global aerosols, it is highly unlikely that direct aerosol effects play any major role here at the surface level.

Potentially, our results may be confounded by sample size effects, given the stochastic nature of storm number in any given year, especially taking into account the systemic effects of oscillations/cycles including ENSO. Large-scale cyclogenesis-related variable outputs and ENSO indices are explored to examine potential mechanisms for this unexpected result, in Chapter 5.

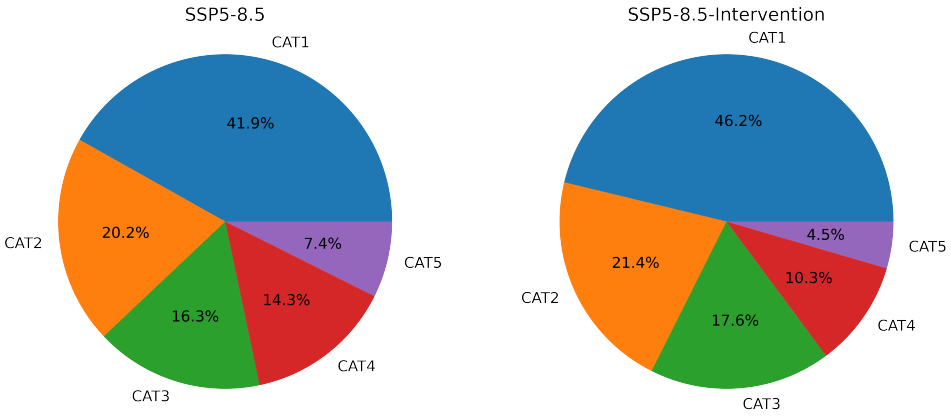

FIG. 4.1. Category Distributions (max lifetime intensity)

On a global scale, however, our results suggest that SAI does not pose major global risks with respect to cyclogenesis and maximum storm intensity. Apart from shifts in basin-scale storm counts, our SAI tempestology appears to combine features of our other two scenarios', without any extraordinary non-linear effects or fundamental shifts in cyclogenesis or storm behavior. Thus, SAI can likely be treated as comparable to other forms of climatic evolution/change, and analyzed in this domain largely on the basis of SSTs and stability measures like CIN/PI.

4.2 BASIN AND LATITUDE DISTRIBUTION

The most notable basin-scale feature of our SSP5-8.5 scenario is a substantial reduction in Atlantic basin TC activity vs. our Control Run. The share of storms occurring in this basin roughly halves, on top of overall reductions in global activity, yielding a net 61% reduction in Atlantic basin storm count (96 vs. 37). This confirms results of similar magnitude found by Bacmeister et al. (2018) in their RCP8.5 experiment as compared with their present day baselines. Notably however, this contradicts the findings

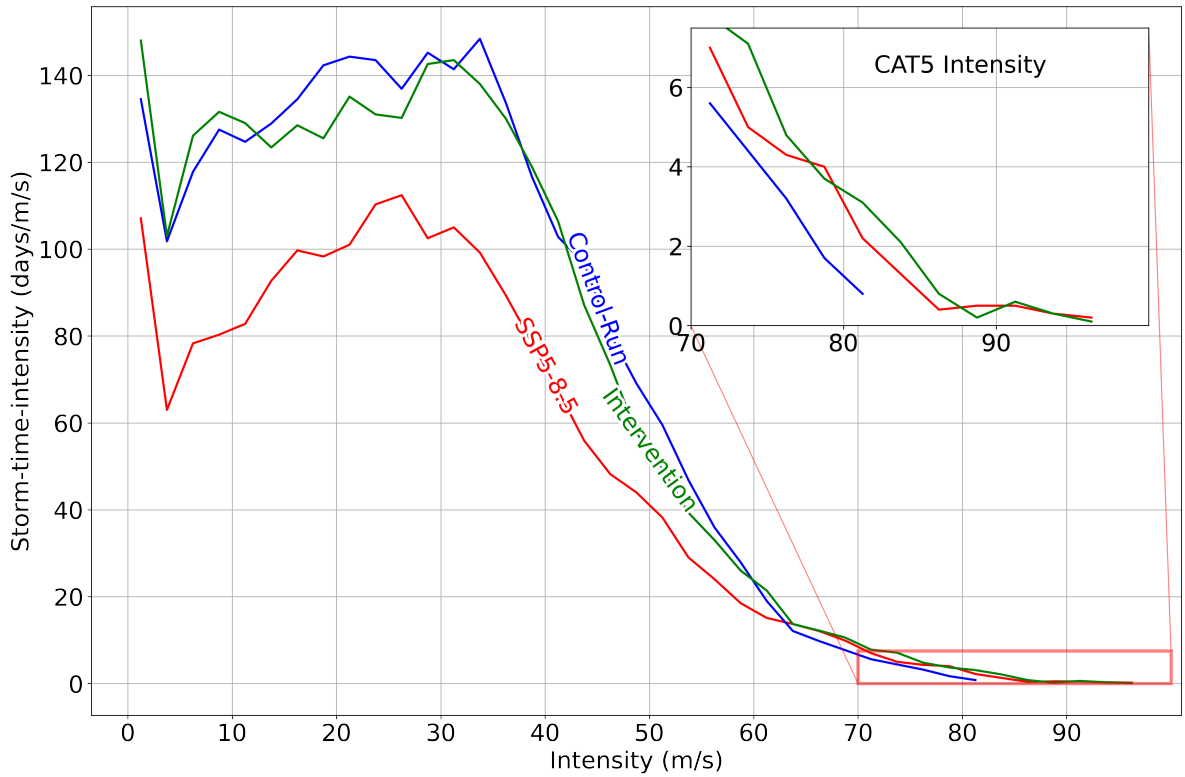

FIG. 4.2. Distribution of WPR-calculated wind intensities for PHAST-generated TC storm tracks (CAT1+). Each storm at each time step constitutes 6 hours of storm-time at its current intensity. Curves extend to maximum observed intensity for each run. Bins are 2.5 m/s wide, with values adjusted to density per m/s unit.

of another set of experiments, Bhatia et al. (2018), our other methods basis paper, who report somewhat increasing numbers of both major storms and overall storm numbers in the Atlantic basin, in both near their near future and end of century simulations, even as frequency does either decrease or remain steady in other regions.

Bacmeister et al. (2018) tentatively attribute the decrease in Atlantic TC activity to El-Niño-type warming exhibited in both their RCP 4.5 and RCP 8.5 experiments, characterized by a significantly warmer east Pacific SST field, and accompanied by enhancements in NW Pacific storms as well. If warming may potentially generate strongly positive mean ENSO states ("permanent El Niño"), and such can lead to such stark reductions in Atlantic and/or other basin activity, this mechanism may then constitute the most significant pathway by which global climate effects global storm distribution.

Also notable in our SSP5-8.5 results is the emergence of activity in the south Atlantic basin absent from our Control Run (and Intervention) data. This novel basin behavior corresponds to increased south Atlantic TC activity seen by Bacmeister et al. (2018) (figure 2). TCs form in this region very rarely

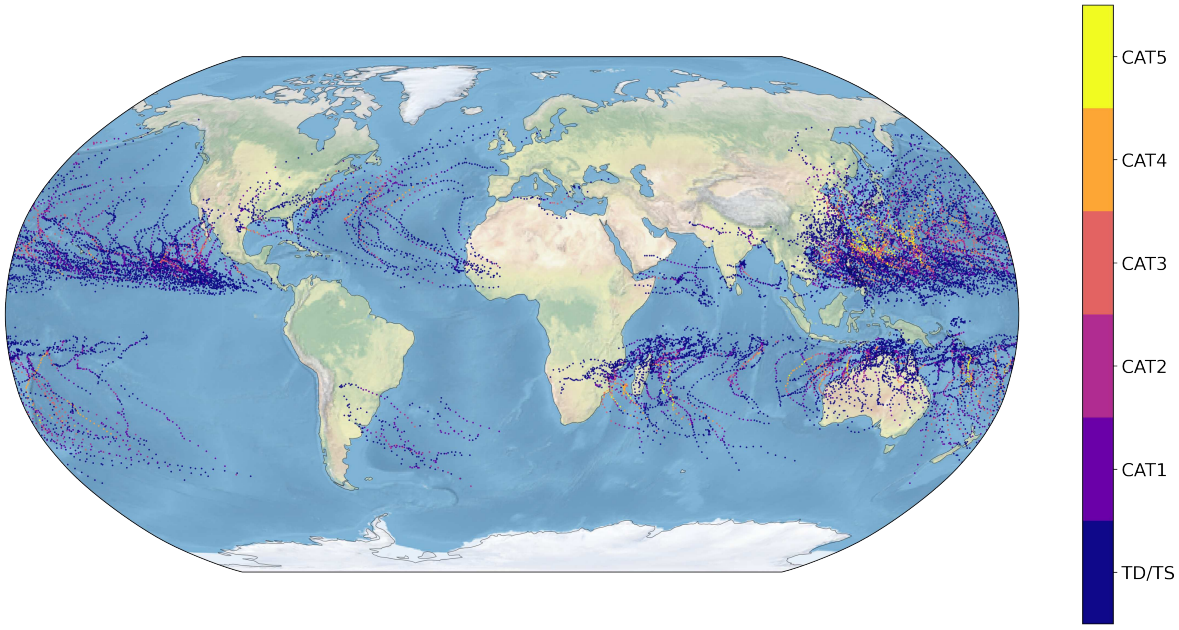

FIG. 4.3. PHAST-generated TC tracks for the years 2090-2099 in our SSP5-8.5 warming scenario. Excludes systems that never achieve CAT1+ intensity based on PHAST WPR.

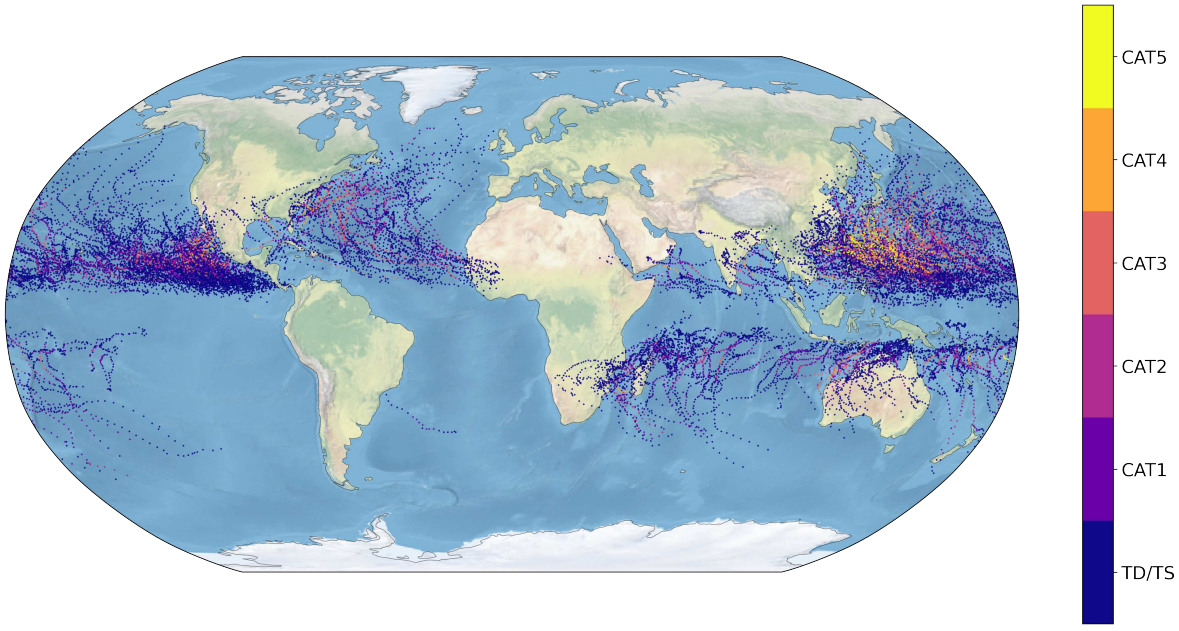

FIG. 4.4. PHAST-generated TC tracks for the years 2090-2099 in our SSP5-8.5-Intervention warming+SAI scenario. Excludes systems that never achieve CAT1+ intensity based on PHAST WPR.

in the observational record, and only once at CAT1+ (Pezza and Simmonds 2006). TCs are generally accepted to not form in this region on account of high tropospheric vertical wind shear, and SSTs below necessary cyclogenesis thresholds. Hurricane Catarina, a potentially unique south Atlantic CAT2 TC

making landfall in Brazil in 2004, occurred in the context of unusually low wind shear in the region, and was connected to a highly positive phase in the Southern Annular Mode (SAM), itself potentially affected by climate change (Pezza and Simmonds 2006).

Hurricane Catarina formed below canonical TC cyclogenesis SSTs, and on that basis would be excluded from our tracking data on the basis of PHAST's 27° C SST threshold. PHAST's detection of storms here may be related to its misattribution of subtropical systems before the introduction of an SST threshold (Methods). But, given that these warming scenario storms are contained firmly in the region where South American TCs occur in real life; and that ocean conditions are significantly more amenable to TC formation than in the present climate, it seems plausible that this result may correspond to a genuinely enhanced risk of TC formation further from the equator than previously, and in regions of the world typically not now associated with such. Shear fields potentially affecting cyclogenesis here are further explored in Bulk Variable Analysis.

Our SSP5-8.5 track data, additionally, includes a very small number of storms meeting TC detection requirements in the Mediterranean. This region already sees TC-like storms, "medicanes" (Lagouvardos et al. 2022), otherwise excluded by our TC SST threshold. However, the detection of valid TCs in this region with warming may indicate the possibility of more truly hurricane-like systems emerging here in the future, or at least highlight possible dangers arising from medicanes forming under conditions with more available thermal energy.

Otherwise, between our Control Run and SSP5-8.5, our global reduction in TC number occurs fairly evenly across the world's major TC basins, with the south Indian basin seeing an especially strong reduction, and very few places observing any increase in TC number (see figure 4.5).

Figure 4.5 also shows major differences between SSP5-8.5-Intervention and both other runs. In magnitude of total warming relative to historical conditions, differences between SSP5-8.5 and SSP5-8.5-Intervention correspond greatly with the BRACE signal explored by Bacmeister et al. (2018) and others, seeking differences in climate/weather risk between RCP8.5 and RCP4.5. Albeit, given the calibration of our chosen SAI paradigm to maintaining important features of the present/pre-industrial climate (Tilmes et al. 2020), important differences will exist in SST and atmospheric temperature patterns between a largely GHG-driven warming of this magnitude, and one achieved through a GHG overshoot paired with any radiation modification scheme.

As compared with unmodified warming, intervention yields higher TC occurrence virtually wherever it exists with any significant density (figures 4.5, 4.6). The number of Atlantic basin storms under

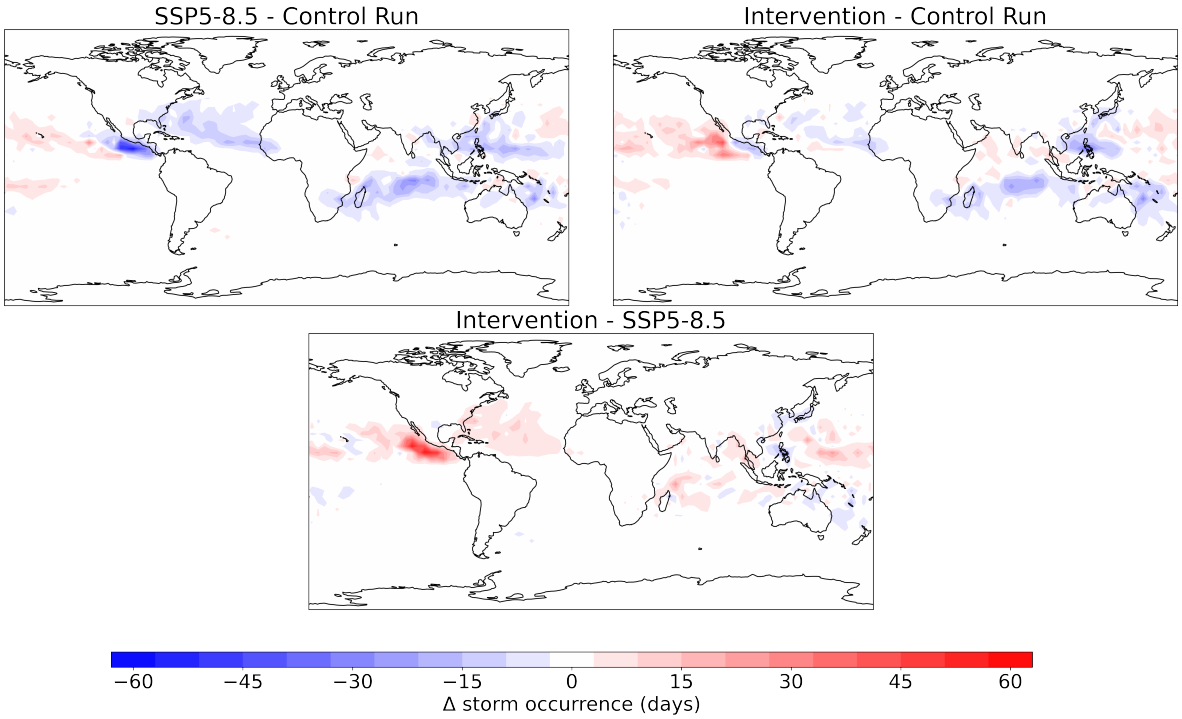

FIG. 4.5. Contour plots of scenario differences in TC (CAT1+) track density. Storm occurrence days are counted on a 4° by 4° grid, based on 6-hour step track positions. Density changes <3 storm days/decade not shown.

intervention is partially restored to historical numbers (69 over the decade), though still represents a significant shift from historical conditions. South Indian basin storms remain consistently suppressed between future scenarios; other, minor basins see small changed in relative storm number share. The most notable basin-scale feature of SSP5-8.5-Intervention, however, is a doubling of storm number in the east Pacific, particularly in waters southwest of the Baja California peninsula. This seemingly leads to substantially increased TC landfall in this general region, and if robust, comprises the most significant enhanced TC hazard posed by this regime of SAI.

Like Atlantic basin suppression, such enhanced eastern Pacific activity, particularly in the basin's western development region, is consistent with strongly positive ENSO (Jien et al. 2015). However, the fact that both of these El Niño responses occur substantially with intervention, but don't consistently correlate across scenarios, indicates a need to examine intermediate mechanisms between ENSO and storm activity, further discussed in Bulk Variable Analysis.

All three of our simulations share roughly similar relative global storm distribution patterns between the northern and southern hemispheres. However, our Intervention case possesses a significantly greater share of NH storms, in line with enhanced east Pacific and north Atlantic activity relative to

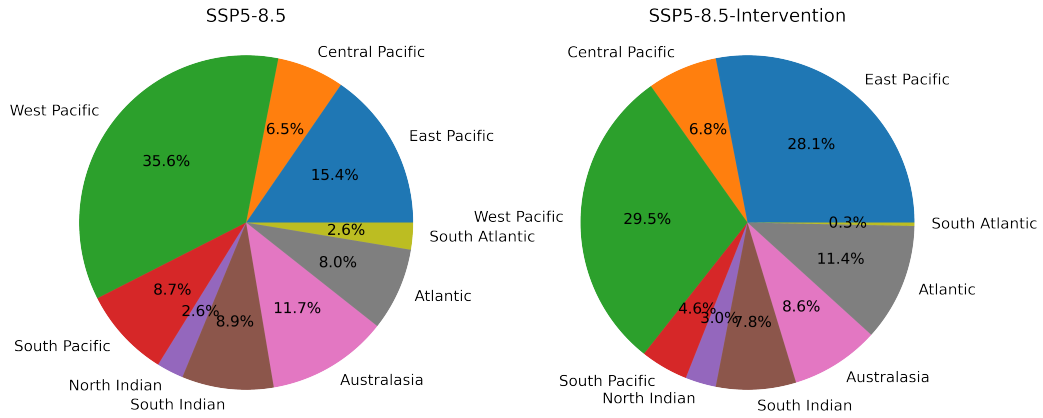

FIG. 4.6. Basin Distributions (system origin)

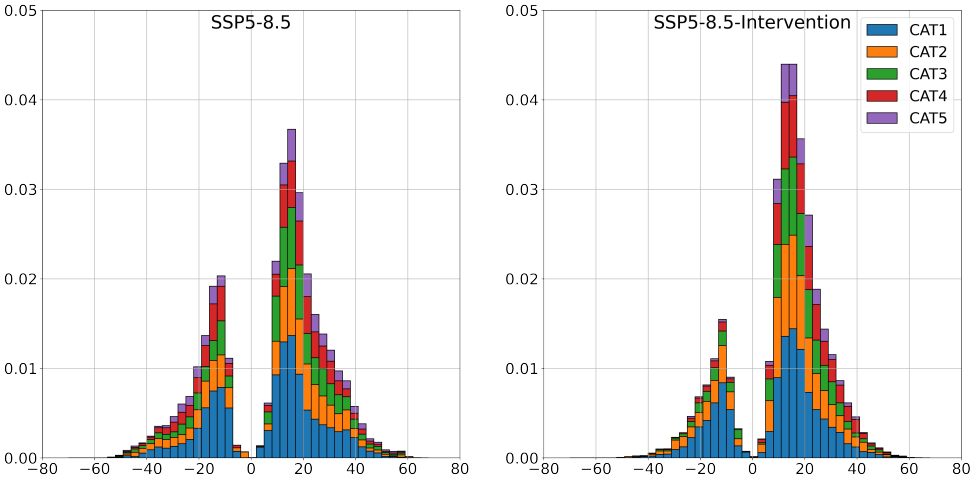

FIG. 4.7. Latitude occurrence distribution by storm category (max lifetime intensity); 6-hourly track data.

SSP5-8.5, paired with nearly across the board suppression in SH basins roughly in line with such. The emergence of our new minor south Atlantic basin in SSP5-8.5 creates a more significant poleward tail in SH track locations, matching a small shift northward in mean NH track positions from the 1990s (20.1° to 20.9°). Expansion of regions conducive to maintaining TC convection should expand track ranges poleward, but storms travelling to temperate zones may experience preexisting or newly powerful shear

leading to their dissolution, regardless of changes in initial cyclogenesis.

Translational speeds in our two future scenarios are largely unchanged from our historical run, with SSP5-8.5 and SSP5-8.5-Intervention having mean TC track speeds of 20.4 and 20.6 km/h, respectively. Mean storm lifetimes however, reduce from 11.2 days in our Control Run to 10.3 and 10.9 days. The reduction in lifetime and thus overall track length with unmodified warming appears to occur largely as a result of more poleward cyclogenesis, unpaired with any significant expansion in where TCs/TC remnants can survive in colder regions. Southern Hemisphere cyclogenesis statistics are changed non-linearly with warming by the enabling of successful south Atlantic cyclogenesis, but mean NH starting TC storm track latitude in the NH shifts from 12.4° in the historical scenario, to 14.5° and 11.8°, respectively, in our warming and intervention cases. Thus, storms forming more poleward will tend to be extinguished by latitudinal/continental features relatively sooner, combining with lowered TC numbers to further reduce global TC occurrence time, if not necessarily storm-related coastal hazards.

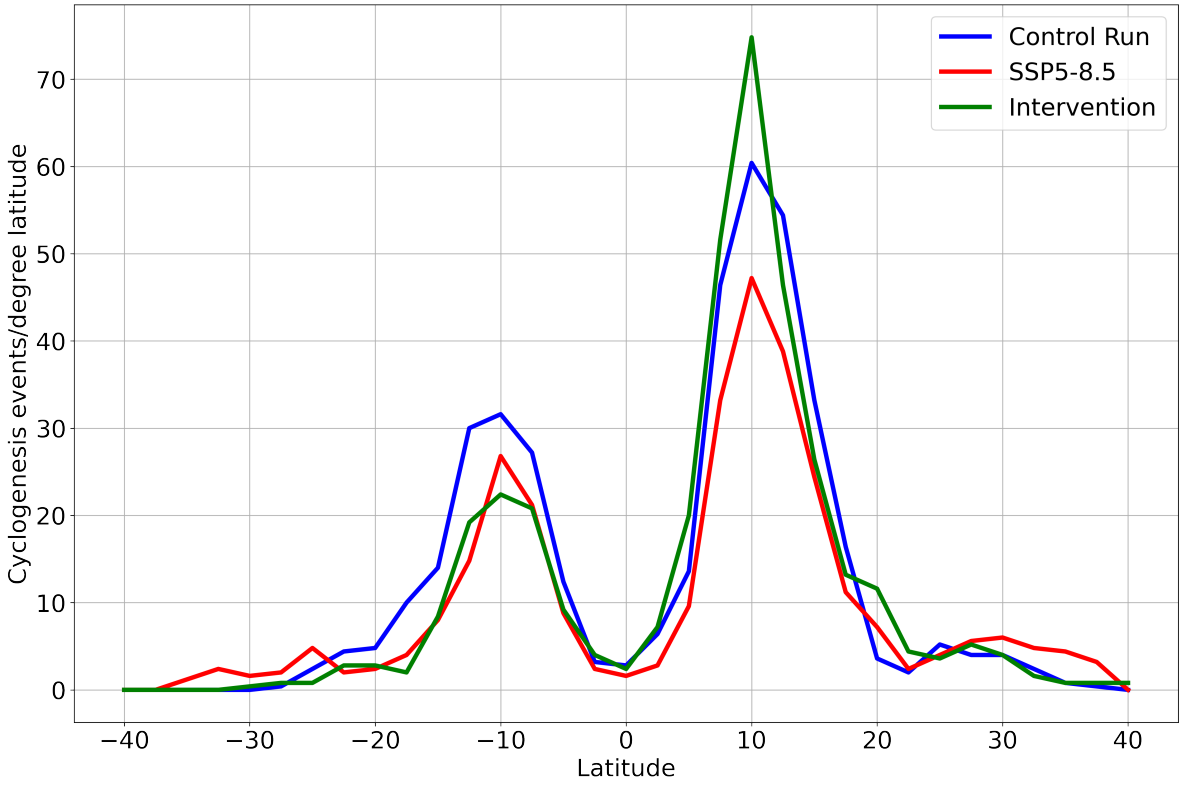

FIG. 4.8. Distribution of starting latitudes of all PHAST-tracked storms (max intensity TS+). Bins are 2.5 ° latitude wide, with values adjusted to density per ° latitude unit.

Expanding our analysis momentarily to include max-intensity TS tracks (figure 4.8), we see that even as the number of cyclogenesis events total declines with warming (from 991 in our historical scenario

to 773 and 921 in our warming and intervention cases), there are greater absolute numbers of such events starting around +/- 25° in each hemisphere. By contrast, storm formation is still about equally suppressed at the equator due to its associated minimum in Coriolis force, with residual equatorial recorded cyclogeneses likely occurring due to especially early lifetime/feature detection as compared with best track data, as discussed in the previous chapter.

Overall, warming will tend to act on TC latitude distributions within basins and/or apart from more specific teleconnections, through changes in cyclogenesis. Despite polar amplification and other developments that could make the mid-latitudes more like the tropics, TC systems are seemingly not able to survive significantly further from the equator than in the historical record, likely on account of persistent limiting factors like mid-latitude shear. Rather, even as increasing tropospheric stratification suppresses storm formation in large parts of the tropics, warmer SSTs enable cyclogenesis in new regions, at increasing frequency in marginal areas, and potentially may even open up a new minor basin.

4.3 Rapid Intensification

Notably, in contrast to Bhatia et al. (2018), warming in our warming scenario produces small, consistent decreases in the share of observed TCs undergoing RI, from 25.3% and 50.4% for CAT1+ and major storms, respectively; to 20.0% and 44.0% in SSP5-8.5; and 23.9% and 51.6% in the Intervention case. The mean max intensities of CAT1+ storms without and with RI, however, stay roughly the same or increase (in both future scenarios), to 48.1 m/s and 62.4 m/s in SSP5-8.5; and 47.7 m/s and 61.3 m/s with Intervention, in contrast to 47.4 m/s and 56.5 m/s in the historical data.

This is somewhat counterintuitive, given the association of RI with increasing storm intensity, and the overall greater share of storms under warming reaching major storm status. However, RI processes may operate through distinct mechanisms/modalities vs. other intensification processes (Judt et al. 2023), and thus storms could in fact grow more intense on average without any increasing frequency of RI. Features like changes in shear may reduce rates of RI significantly more than they effect intensification overall, reflecting the multiple competing mechanisms by which shear, cyclogenesis and heat engine effects combine to yield new patterns of storm occurrence and intensity.

4.4 Seasonality

Broadly, in all scenarios, NH and SH TC occurrence maintain the same basic relationships with hemispheric seasonality. TC formation remains dependent on meeting minimum threshold SSTs, which are most present in late summer/early autumn, as well as/in relation to other cyclogenesis enabling

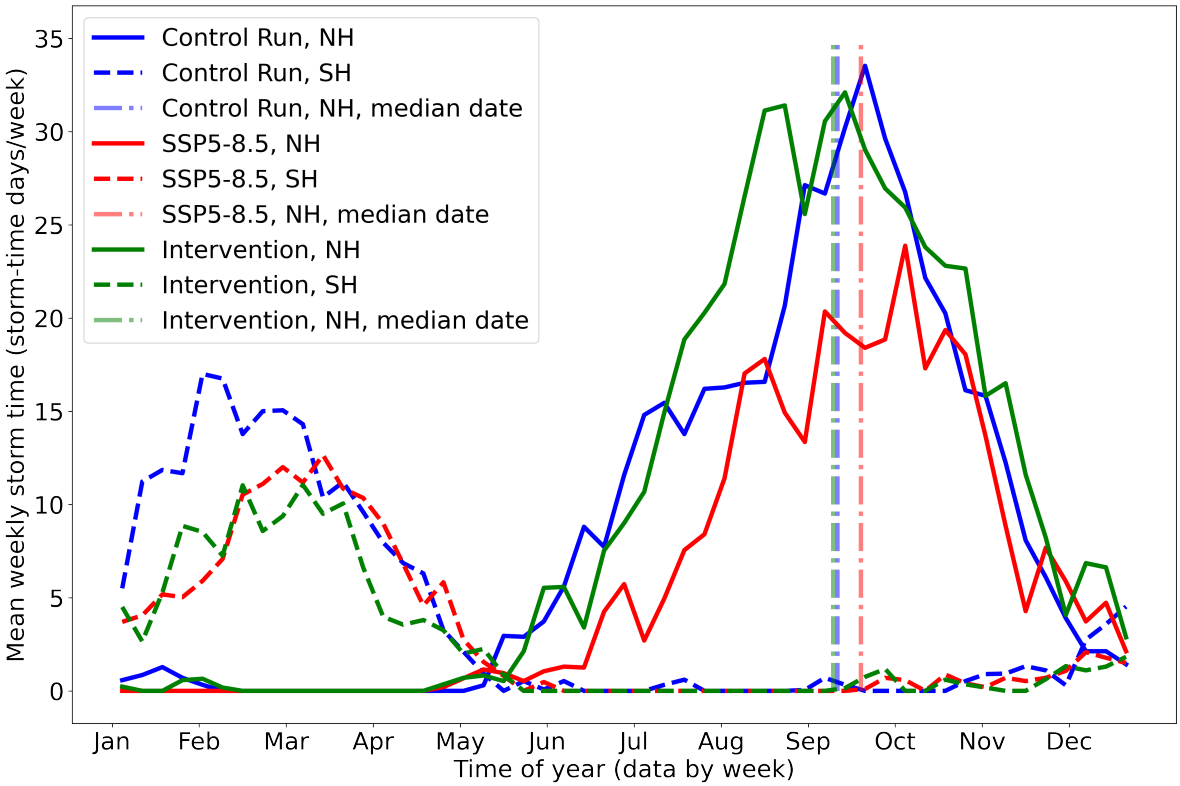

FIG. 4.9. Storm occurrence density by time of year, cumulative over full scenario run periods. Binned approximately by week (365 days/52 weeks). Storm occurrences counted in 6-hour intervals.

factors.

With warming, mean and median storm occurrence time are delayed further in each hemispheric storm season (discussed further in Global Temperature Patterns). This change in timing however cannot be completely disentangled from basin-scale effects, given differing basin seasonal patterns paired with relative changes in basin TC share. Given the data limitations of this study, and the high variability of storm track time-occurrence within a given basin in any given year, any such regional seasonality findings will necessarily be low-confidence. But, overall hemispheric trends reveal that despite rising global SSTs, under warming it becomes increasingly difficult for early-season TCs to arise and intensify across the world. By contrast, late-season TC occurrence in both hemispheres may be largely unaffected by warming or warming limited by intervention, or even increase despite sharp drops in all-season activity overall.

Given that storm lifetimes are not, on net, increasing, this shift must be driven in large part by changes in cyclogenesis favorability, in particular by those in limiting factors acting counter to rising SSTs, explored further in Chapter 5.

CHAPTER 5

BULK VARIABLE ANALYSIS

5.1 GLOBAL TEMPERATURE PATTERNS

Forced by our WACCM-provided SSTs, but with dynamically calculated land temperature patterns, our Control Run, SSP5-8.5 and SSP5-8.5-Intervention scenarios see mean global temperatures over their respective decade runs of 15.3°, 20.9°, and 16.3° C. By itself, changes in global temperature patterns between our Control Run and SSP5-8.5 scenarios would likely yield significant increases in both global storm number and intensity. All major TC regions see substantial warming (although the greatest warming trends are confined to the Arctic and Antarctic). The number of monthly location-time points on our interpolated .25° grid exceeding the 27° threshold increases X1.9 with warming, and regions of ocean with cyclogenesis-enabling temperatures expand in both time and space.

Due to other effects of a warming ocean/ice caps, including sea level rise, coastal ecosystem shifts, and a greater atmospheric capacity to hold moisture (Knutson et al. 2020), TCs may also pose significantly more risk to coastal communities regardless of changes in their formation and dynamics.

Due to uncertainties in the mechanisms controlling TC formation (Emanuel 2022), it is difficult to say quantitatively how much warming SSTs should change TC patterns by themselves. Some features of the SSP5-8.5 tempestology are suggestive of an expansion of cyclogenesis caused by SST changes relative to Control Run. These include poleward movement of storm track (CAT1+) starting latitudes (from mean 12.4° to 14.5° in the NH, and -11.8° to -13.2° in the SH).

As well, the mean date of such NH storms' place-time occurrences is delayed 10.7 days further into the season, from September 6th to September 17th, and the median date is delayed 8.25 days, from September 10th to September 18th. Higher SSTs combined with lower overall storm numbers, especially/largely early in each hemispheric season, indicate higher SST thresholds typically reached later in the season perhaps becoming necessary to break through greater cyclogenesis barriers. It is evident, then, from both first principles and observed interactions in our model outputs, that rising SSTs in our warming world are acting counter to changes in vertical stability or other factors acting to suppress TC activity, and overall shifts in global storm patterns arise from a balance of these.

Given countervailing trends in vertical stability and shear, however, the clearest example of SST-driven changes in cyclogenesis is likely in our newly populated south Atlantic basin in SSP5-8.5. Despite local increases in stability and intensification of already strong shear, TC activity rises from virtually

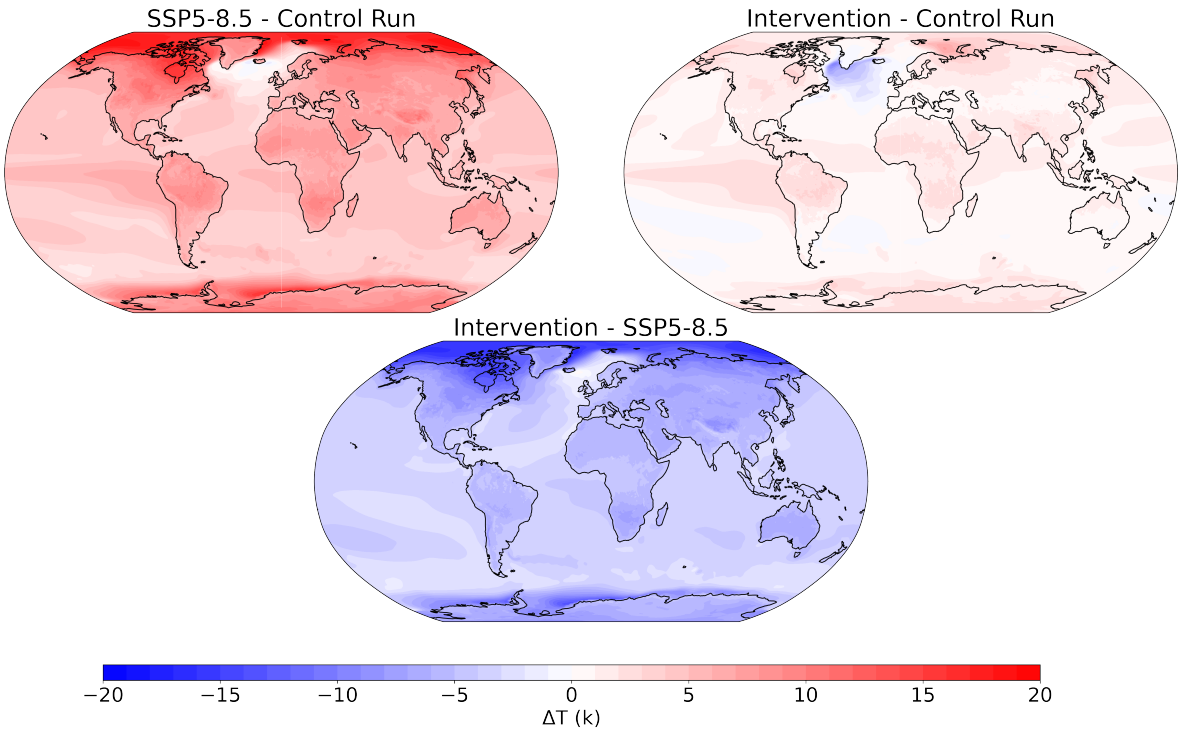

FIG. 5.1. Contour maps of change in mean decadal temperature between pairs of scenarios. Contours occur in increments of 1° K. Note prominent North Atlantic warming hole features.

nothing in the other two cases, to on the order of 1 CAT1+ storm per year. Given its sharp divergence from current tempestologies, this result is necessarily low certainty in the absence of corroborating non-model evidence. But it is in line with our overall understanding of cyclogenesis, and presents perhaps the most novel potential hazard arising from TCs in a warming climate.

5.2 ENSO

As discussed in Introduction, it is possible that climate change may give rise to shifts in current ENSO patterns (Callahan et al. 2021), which may be a primary mechanism by which climate interacts with TCs.

Challenges in studying ENSO as it occurs in our model runs (primarily, in SST data from our forcings) include the limitations of common indices/metrics like ONI and similar, which are dependent on baseline climatologies (NOAA 2024a). Given the relatively short spans of our model runs, and their non-continuity in time from each other, we have turned to an alternative, history-agnostic ENSO index, the ENSO Longitudinal Index (ELI) (Williams and Patricola 2018). For each month of our climatological data, we have computed ELI by finding the mean longitude of Pacific SST points warm enough to permit convection, occurring between +/- 5° latitude, as defined by Williams and Patricola (2018). This index

allows us to compare ENSO behavior between radically different climate regimes, regardless of shifts in baseline SSTs that may otherwise obscure important new modalities.

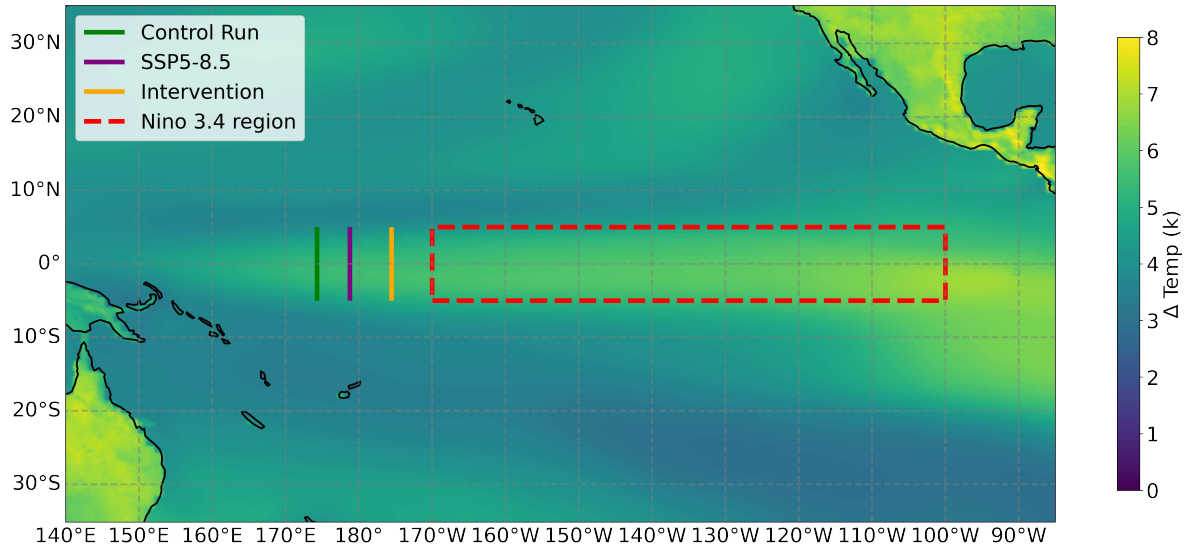

FIG. 5.2. Mean all-run ELI longitude for each scenario, mapped against Niño 3.4 region used in calculating ONI based on SST anomalies.

FIG. 5.3. Monthly ELI longitudes, indexed from start of each scenario

From the perspective of mean SST changes between our Control Run and two future scenarios (figure 5.2), the Niño 3.4 and broader equatorial cold tongue region warms at a substantially higher rate than adjacent regions of ocean, including relative to the western Pacific. This is in line with a substantial

weakening of ocean upwelling in the cold tongue region, and indicates a version of permanent El Niño occurring by the end of the century with both advanced warming and warming offset by SAI.

Through the lens of our ELI index (figure 5.2, figure 5.3), while mean ENSO intensity does substantially increase between our Control Run and both future scenarios, this is driven by a shift toward much more powerful positive-ENSO (El Niño) events. These events regularly push the calculated mean longitude of convection in the Pacific well east of anything observed in the historical simulation, and through El Niño's effects on vertical wind shear and stability measures (Arpe and Leroy 2009), could perhaps entirely explain our observed future drops in Atlantic TC activity. Such an association would be in line with other TC modeling work showing a strong effect of both ENSO state and intensity on Atlantic TC activity in other GCMs (Wang et al. 2014), as well as in the observational record.

The degree of storm activity enhancement in the east Pacific with intervention could potentially be a function of the much greater strength of El Niño events observed in that climate trajectory as compared with SSP5-8.5 (figure 5.3), including unprecedentedly powerful El Niño events in simulated 2091 and 2096 (compare to long-term historical index values in Williams and Patricola (2018)). These may interact non-linearly with other climate features to create periods of higher storm activity, or higher ENSO intensities may merely be less damped in their effect on this basin by separately arising changes in other cyclogenesis variables. ENSO may particularly influence TC activity in this region through higher SSTs and changes in vertical shear (Jien et al. 2015), which occur on top of mean climatologies and thus provide an opportunity for this difference in scenario responses.

Work by Mueller et al. (2024) using a direct TC modeling approach in WRF, finds that even in an overall more El Niño-like future climate, year-to-year variations in ENSO indices are still predictive of Atlantic TC activity, even as long-term conditions further suppress such. Thus, whether our ENSO results are interpreted as a shift toward permanent El Niño conditions, as a tendency toward substantially stronger El Niño events, or some combination of such, ENSO and its effects on Atlantic basin shear and vertical stability are consistent with our TC observations, with intermediate mechanics discussed in Vertical Stability and Shear.

5.3 Vertical Stability

We have focused our analysis of vertical stability on Convective Inhibition (CIN), a measure of the energy required for surface parcels to reach the level of free convection. Broadly, higher values of CIN should make it substantially more difficult for cyclogenesis to occur, by preventing upward convection

from reaching a great enough height to start a robust TC heat engine.

For purposes of studying shifts in CIN as they relate to cyclogenesis, we have produced maps of monthly mean values for the three months comprising peak hemisphere-wide TC occurrence in both the NH and SH, when cyclogenesis is most likely to occur.

Our most notable NH season finding is a profound intensification in mean CIN values in the eastern Atlantic basin area, extending prohibitive CIN levels to large new parts of the basin's main cyclogenesis areas. This occurs in both future scenarios, albeit much more strongly without intervention. Although our PHAST-generated Atlantic tracks often begin over west Africa itself, important steps in cyclogenesis/early intensification are still occurring in this oceanic high-CIN region in line with observations. Overall, given the contributions of CIN-related terms in formulations like the Genesis Potential Index (Camargo et al. 2007), the profound changes in such observed here are likely to be the primary, directly controlling variable in determining Atlantic TC activity in our experiments.

Additionally, changes in CIN off western North America may serve to enhance/suppress TC intensification on intersecting tracks, likely reflected in differences in east Pacific storm activity between SS5-8.5 and SSP5-8.5-Intervention. But given how different storm activity is in this region between our Control Run and Intervention cases, despite similar CIN patterns, this is likely not the full story of primary TC controls here.

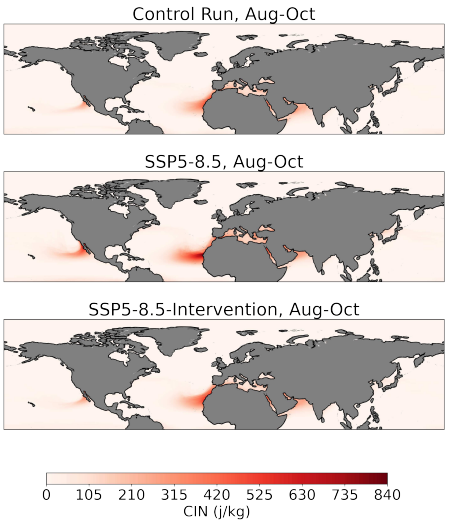

FIG. 5.4. Mean decadal, storm-season mean CIN values for the NH.

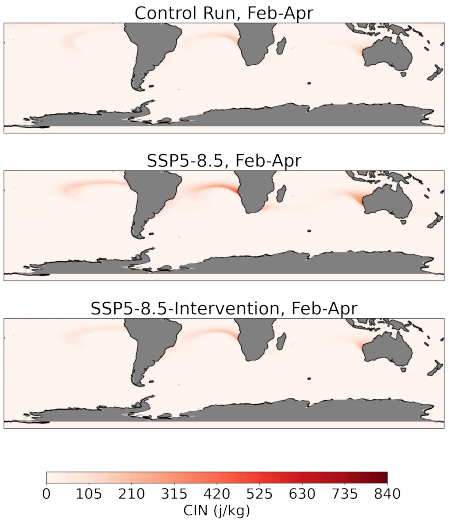

FIG. 5.5. Mean decadal, storm-season mean CIN values for the SH. Colorbar calibrated to NH all-scenario maximum.

In the west Pacific, though changes in CIN are substantially smaller in the Atlantic and elsewhere (figure 5.6), significant increases can be seen in the main development region between our SSP5-8.5 and other two scenarios. Given SSP5-8.5's relative dearth of storms here in the world's most significant basin, and the lack of a strong local forcing created by vertical shear, this tongue of newly increased CIN

generated by warming SSTs is likely responsible for much of the reduction in global storm numbers in this scenario overall.

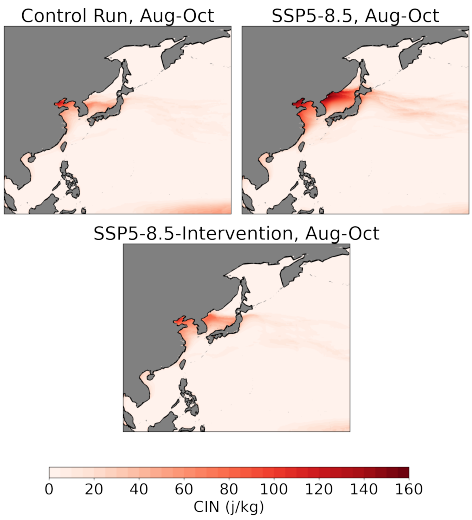

FIG. 5.6. Mean decadal, storm-season mean CIN values for the west Pacific region. Note eastward tongue of higher inhibition in SSP5-8.5. Colorbar calibrated to local all-scenario maximum.

Future changes in CIN during the SH season may potentially intersect with parts of the broader Australasia storm development region, particularly in SSP5-8.5. But this appears unlikely to be a significant determinant of SH activity, with our CIN results here likely pointing to other factors being dominant.

Overall, changes in CIN are likely playing a fundamental part in mediating cyclogenesis and intensification patterns in the NH's three major basins. However, they are insufficient to explain all variation between scenarios, and in the SH may not be as broadly explanatory relative to our other main cyclogenesis control variables, shear and SSTs.

5.4 SHEAR

Looking first at NH shear (magnitude 200 hPa - 850 hPa vectors) (figure 5.6), highly apparent is profound differences in east Pacific basin shear between our Control Run and SSP5-8.5 scenarios, and between SSP5-8.5 with and without intervention. These occur in the main development region, are likely influenced by ENSO, and in interaction with shifts in SST and vertical stability (discussed further in East Pacific Synthesis). Altogether, this result, along with higher trackway CIN in SSP5-8.5, likely explains the greater incidence of storms here with SAI in spite of higher SSTs otherwise.

Increases in Atlantic development area shear in both future scenarios are in line with expectations given highly increased ENSO indices. These operate in the same direction as CIN in influencing future activity in the basin, and help explain the extreme degree of Atlantic TC suppression seen here and ultimately driven through these intermediate mechanisms by permanent El Niño.

In the SH, given already high levels of vertical shear across basins, substantial increases in such, and the predicted exponential nature of genesis suppression with shear (Camargo et al. 2007), can more than explain substantial reduction in SH storm activity in both future scenarios, including the sharp NH-SH divergence in activity levels seen in SSP5-8.5-Intervention (figure 4.7).

5.5 East Pacific Synthesis

Trends between our scenarios in the east Pacific TC basin potentially most exemplify the complexity of cyclogenesis controlling factors, and thus the inherent uncertainties in predicting TC behavior with warming.

Despite observed associations between El Niño events, which occur powerfully in SSP5-8.5, and east Pacific storm activity (Jien et al. 2015), this simulation sees an overall reduction in storm number in this basin. Warming with intervention, by contrast yields substantial increases in activity putting this basin on par with the western Pacific in global TC share.

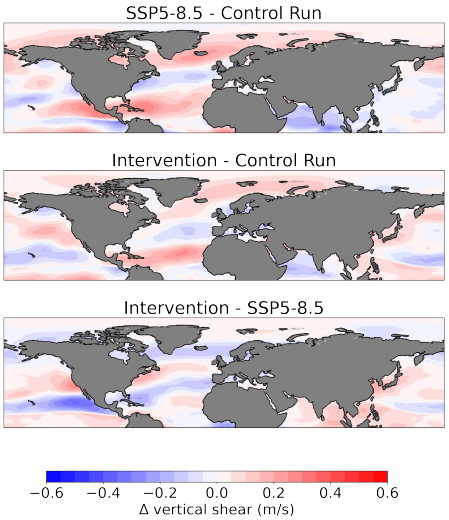

FIG. 5.7. Change in mean decadal, NH storm-season Euclidean shear magnitude between pairs of scenarios. Magnitudes calculated based on monthly mean U, V values for 200, 850 hPa, differences taken between magnitudes.

As shown by a close-in view of main-season SSTs in this region, temperatures are already, in historical data, consistently above theoretical thresholds for TC formation, and in both future scenarios well exceed these. This is partly a function of overall global temperature increases, and partly a result of strongly elevated ENSO indices in both. In either future, all else being equal, this would constitute a positive forcing on TC number.

In terms of local vertical stability changes, in line with parts of other NH basins, SSP5-8.5 sees a substantial expansion of the high-CIN region in the northern part of many typical storm tracks here. While having less of an effect on cyclogenesis itself, this likely serves to reduce the number of storms able to intensify sufficiently as they translate northwest to ever reach CAT1 or become detectable to our algorithm altogether. By contrast, despite its own local (substantially weaker) SST increases, our Intervention case does not experience a similar CIN effect.

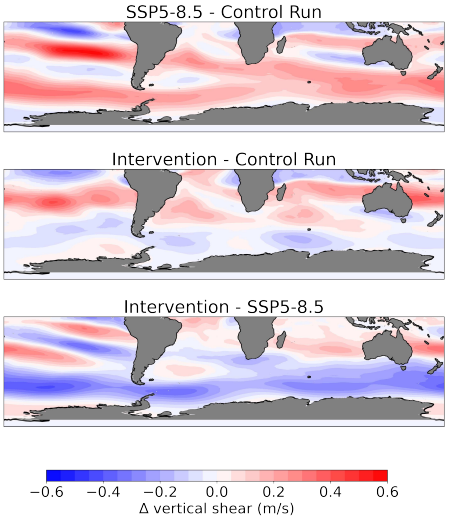

FIG. 5.8. Change in mean decadal, SH storm-season Euclidean shear magnitude between pairs of scenarios.

The largest differentiating factor here, however, appears likely to be distinct patterns of shear. On top of already fairly significant shear levels in this region, SSP5-8.5 sees very large increases in shear (by

NH standards) in the main cyclogenesis region, while between our historical and intervention runs, there's almost no change. Given what's theoretically understood about cyclogenesis, this increase in shear with climate change could more than cancel out any enhancements due to increased SSTs and ENSO effects more broadly, and is likely the primary explanation for our divergence between climate futures here.

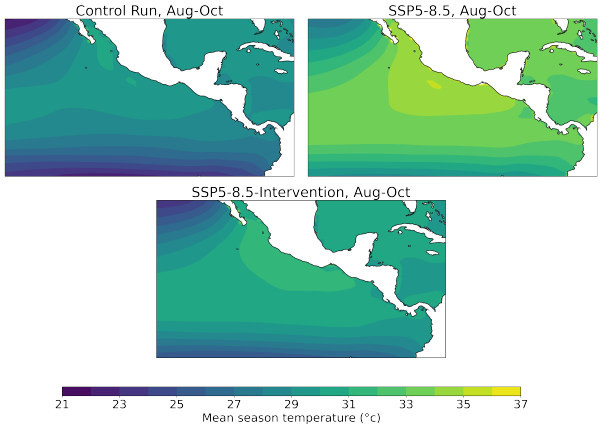

FIG. 5.9. Mean decadal SSTs for east Pacific main development region. Note intensification of Eastern Pacific Warm Pool in future scenarios.

While ENSO is a dominant explanation for many changes in TC distribution going into our future scenarios, competing climate effects may serve to interfere with this signal. In making predictions about strong basin-scale TC activity changes for any given climate trajectory, the strength of forecasts may be highly dependent on the robustness of ENSO modeling. Yet, ENSO indices are not fully determinative even in high-sensitivity regions. And given multiple competing effects, our understanding of climate-TC dynamics for the east Pacific basin, home as it is to many of the world's most powerful storm systems, may necessarily remain more contingent than elsewhere.

CHAPTER 6

CONCLUSIONS

TCs comprise perhaps the most destructive mesoscale weather phenomenon, and thus represent an important target for GSRM-based research occurring at the intersection of climate and weather. With advances in high-resolution modeling, it has become possible to directly model TCs in global simulations in ways that capture important aspects of their relationship with climate, as well as capture important elements of their internal dynamics.

In this paper, we have applied paradigms and existing data sets (Tilmes et al. 2020) from the study of climate interventions, and paired them in new ways with techniques to track TCs occurring natively in high-resolution global climate models. In so doing, we have yielded novel results analyzing for the first time, GSRM TC physics under a realistic, specific climate intervention scenario, algorithmically controlled SAI.

In the course of trying to quantify TC behavior in GCM runs at our chosen resolution, and compare such to real-world observations, we have significantly adapted and borrowed from established existing TC-tracking algorithms (Vitart et al. 1997; Han and Ullrich 2024). In so doing, we have moved away from a focus on model native wind speeds as a measure of intensity and development state, given inherent resolution limitations on such (Davis 2018). Rather other properties, like central pressure and SSTs with more gradual variation in time and space, may be much stronger as fundamental diagnostics of storm nature. Other changes have more simply sought to help capture the dynamics of GSRM TCs occurring densely in time and space, and we believe have largely eliminated earlier miscounts/false negatives arising from feature proximity.

We have found that, with such pressure- and temperature-based TC tracking heuristics, tropical storm behavior in EarthWorks exhibits high fidelity with best-track data. Our model captures important controls on TC number and intensity, and this work helps demonstrate the potential value of studying mesoscale climate-weather interactions using GCMs at this and even greater resolutions. We have confidence that the results of our future scenario experiments, then, highlight salient causal links between the climate properties emergent in our forcings data sets and the storm behavior that could result from such.

In trying to understand how global TC behavior will respond to climate change, and attempts to ameliorate such, several potential mechanisms become important to determining outcomes in each

basin, but notably may not all act in the same direction. This has the effect of substantially reducing the certainty of any forecasts of future TC patterns, particularly given present limitations of available computational power, and persistent issues in how GSRM's represent TC's even at finer grid spacings at the limits of computational possibility (Judt et al. 2021).

Perhaps our most notable finding here is that, given a realistic, targeted implementation of climate intervention through algorithmically-controlled SAI, tempestological outcomes in each basin can behave in a highly non-linear fashion given different degrees of net warming. That is, the properties and distribution of storms in our SAI climate is not, fundamentally, intermediate between those in historical and advanced warming scenarios. Rather, such intervention may yield significant novel risks (say, extremely magnified east Pacific storm activity), even while bringing local climate variables back below thresholds for others (the emergence of a significant south Atlantic basin in SSP5-8.5).

Among the principal limitations on this work has been that presented by available computational power. All climate-modeling studies face an inherent trade off between simulation time and model resolution. In our decisions to run EarthWorks for 30 total years, split among 3 scenarios at ∼30 km spacing, we have utilized the resources available to us to produce as much salient GRSM storm-resolving data as possible. The relative usefulness of our pressure-based storm intensity metrics used here derives in large part from the inherent limitations of direct TC modeling at this resolution. Going forward, future research studying the impact of SAI and other climate interventions on TCs and other mesoscale features would potentially gain considerable robustness from longer simulation run times and/or finer grid spacings. This is especially true if these are combined with model dynamics/parameterization improvements that create more realistic TCs and other mesoscale features (Nardi et al. 2022), allowing us to study GSRM storms in greater individual detail and output small-scale metrics like TC precipitation and internal dynamics more grounded in reality.

The other main avenues for further work here include broadening the range of considered climate intervention scenarios. Different strategies for implementing SAI with alternate climate priorities may yield substantially distinct SST patterns. Altogether different intervention technologies could vary in this way, while also introducing geochemical (Kravitz et al. 2013) or other effects that act on TC distribution beyond the mechanisms considered here. No set of chosen scenarios could capture every possible pattern of SST and other TC-affecting variables. But, a greater variety of simulations that radically alter the present Earth's basic thermodynamics could help untangle possible mechanisms that control TC behavior at this scale of change. Of particular value for understanding future Atlantic basin behavior

would be model runs either organically or intentionally exhibiting significantly lower ENSO indices than arose in our future scenarios.

Broader high-resolution intervention modeling would also contribute to understanding TCs as they occurred in the distant past, and future GSRM paleoclimate modeling could in turn help inform our expectations of both warmed and engineered worlds.

Given the scale and persistence of other hazards at play in considering advanced warming scenarios and possible interventions, including sea level rise, heat waves, drought, etc., TCs are unlikely to comprise a determinative factor in informing specific geoengineering/emissions policy. But, they represent an important locus through which global climate can have severe local impacts, with their stochastic and emergent nature substantially complicating our ability to predict and adapt to their behavior in the long term. And thus, as our broader climate trajectory gradually solidifies, it remains important to remember that TCs and other highly downstream phenomena may behave unexpectedly, and non-linear shifts in such may constitute important contours of the climate future.

REFERENCES

Aquila, V., C. Baldwin, N. Mukherjee, E. Hackert, F. Li, J. Marshak, A. Molod, and S. Pawson, 2021: Impacts of the eruption of mount pinatubo on surface temperatures and precipitation forecasts with the nasa geos subseasonal-to-seasonal system. *Journal of Geophysical Research: Atmospheres*, **126 (16)**, e2021JD034 830.

Arpe, K. and S. A. Leroy, 2009: Atlantic hurricanes—testing impacts of local ssts, enso, stratospheric qbo—implications for global warming. *Quaternary International*, **195 (1)**, 4–14.

Atkinson, G. D. and C. R. Holliday, 1977: Tropical cyclone minimum sea level pressure/maximum sustained wind relationship for the western north pacific. *Monthly Weather Review*, **105 (4)**, 421 – 427.

Bacmeister, J. T., K. A. Reed, C. Hannay, P. Lawrence, S. Bates, J. E. Truesdale, N. Rosenbloom, and M. Levy, 2018: Projected changes in tropical cyclone activity under future warming scenarios using a high-resolution climate model. *Climatic Change*, **146 (3)**, 547–560.

Bacmeister, J. T., M. F. Wehner, R. B. Neale, A. Gettelman, C. Hannay, P. H. Lauritzen, J. M. Caron, and J. E. Truesdale, 2014: Exploratory high-resolution climate simulations using the community atmosphere model (cam). *Journal of Climate*, **27 (9)**, 3073 – 3099.

Bellamy, R., J. Chilvers, N. E. Vaughan, and T. M. Lenton, 2012: A review of climate geoengineering appraisals. *WIREs Climate Change*, **3 (6)**, 597–615.

Benton, B. N., M. J. Alessi, D. A. Herrera, X. Li, C. M. Carrillo, and T. R. Ault, 2022: Minor impacts of major volcanic eruptions on hurricanes in dynamically-downscaled last millennium simulations. *Climate Dynamics*, **59 (5)**, 1597–1615.

Bhatia, K., G. Vecchi, H. Murakami, S. Underwood, and J. Kossin, 2018: Projected response of tropical cyclone intensity and intensification in a global climate model. *Journal of Climate*, **31 (20)**, 8281 – 8303.

Cai, W., et al., 2018: Increased variability of eastern pacific el niño under greenhouse warming. *Nature*, **564 (7735)**, 201–206.

Callahan, C. W., C. Chen, M. Rugenstein, J. Bloch-Johnson, S. Yang, and E. J. Moyer, 2021: Robust decrease in el niño/southern oscillation amplitude under long-term warming. *Nature Climate Change*, **11 (9)**, 752–757.

Camargo, S. J., K. A. Emanuel, and A. H. Sobel, 2007: Use of a genesis potential index to diagnose enso

effects on tropical cyclone genesis. *Journal of Climate*, **20 (19)**, 4819 – 4834.

Danabasoglu, G., 2019a: Ncar cesm2-waccm-fv2 model output prepared for cmip6 cmip historical. Earth System Grid Federation, URL `https://doi.org/10.22033/ESGF/CMIP6.11298`, doi: 10.22033/ESGF/CMIP6.11298.

Danabasoglu, G., 2019b: Ncar cesm2-waccm model output prepared for cmip6 scenariomip ssp585. Earth System Grid Federation, URL `https://doi.org/10.22033/ESGF/CMIP6.10115`, doi: 10.22033/ESGF/CMIP6.10115.

Davis, C. A., 2018: Resolving tropical cyclone intensity in models. *Geophysical Research Letters*, **45 (4)**, 2082–2087.

Emanuel, K., 2007: Environmental factors affecting tropical cyclone power dissipation. *Journal of Climate*, **20 (22)**, 5497 – 5509.

Emanuel, K., 2022: The enduring enigma of tropical cyclone formation (session 3, 1:39:00). URL `https://web.mit.edu/webcast/eaps/s22/2/`, Live Webcast/Video Archive.

Emanuel, K., C. DesAutels, C. Holloway, and R. Korty, 2004: Environmental control of tropical cyclone intensity. *Journal of the Atmospheric Sciences*, **61 (7)**, 843 – 858.

Emanuel, K. and D. Nolan, 2004: Tropical cyclone activity and the global climate system. *26th Conference on Hurricanes and Tropical Meteorology*, AMS.

Emanuel, K., S. Solomon, D. Folini, S. Davis, and C. Cagnazzo, 2013: Influence of tropical tropopause layer cooling on atlantic hurricane activity. *Journal of Climate*, **26 (7)**, 2288 – 2301.

Emanuel, K., M. Velez-Pardo, and T. W. Cronin, 2023: The surprising roles of turbulence in tropical cyclone physics. *Atmosphere*, **14 (8)**.

Emanuel, K. A., 1988: The maximum intensity of hurricanes. *Journal of Atmospheric Sciences*, **45 (7)**, 1143 – 1155.

Frank, W. M. and E. A. Ritchie, 2001: Effects of vertical wind shear on the intensity and structure of numerically simulated hurricanes. *Monthly Weather Review*, **129 (9)**, 2249 – 2269.

Fujiwhara, S., 1921: The natural tendency towards symmetry of motion and its application as a principle in meteorology. *Quarterly Journal of the Royal Meteorological Society*, **47 (200)**, 287–292.

Han, Y. and P. Ullrich, 2024: The system for classification of low-pressure systems (syclops): An all-in-one objective framework for large-scale datasets. *ESS Open Archive*.

Haywood, J. M., A. Jones, N. Bellouin, and D. Stephenson, 2013: Asymmetric forcing from stratospheric aerosols impacts sahelian rainfall. *Nature Climate Change*, **3 (7)**, 660–665.

Heck, V., D. Gerten, W. Lucht, and L. R. Boysen, 2016: Is extensive terrestrial carbon dioxide removal a 'green' form of geoengineering? a global modelling study. *Global and Planetary Change*, **137**, 123–130.

Hersbach, H., et al., 2020: The era5 global reanalysis. *Quarterly Journal of the Royal Meteorological Society*, **146 (730)**, 1999–2049.

Hodges, K., A. Cobb, and P. L. Vidale, 2017: How well are tropical cyclones represented in reanalysis datasets? *Journal of Climate*, **30 (14)**, 5243 – 5264.

Holland, G., 2008: A revised hurricane pressure–wind model. *Monthly Weather Review*, **136 (9)**, 3432 – 3445.

Holliday, C. R. and A. H. Thompson, 1979: Climatological characteristics of rapidly intensifying typhoons. *Monthly Weather Review*, **107 (8)**, 1022 – 1034.

IPCC, 2021: *Summary for Policymakers*, 3-32. Cambridge University Press, Cambridge, United Kingdom and New York, NY, USA, doi: 10.1017/9781009157896.001.

Irvine, P., K. Emanuel, J. He, L. W. Horowitz, G. Vecchi, and D. Keith, 2019: Halving warming with idealized solar geoengineering moderates key climate hazards. *Nature Climate Change*, **9 (4)**, 295–299.

Jien, J. Y., W. A. Gough, and K. Butler, 2015: The influence of el niño–southern oscillation on tropical cyclone activity in the eastern north pacific basin. *Journal of Climate*, **28 (6)**, 2459 – 2474.

Jing, R., N. Lin, K. Emanuel, G. Vecchi, and T. R. Knutson, 2021: A comparison of tropical cyclone projections in a high-resolution global climate model and from downscaling by statistical and statistical-deterministic methods. *Journal of Climate*, **34 (23)**, 9349 – 9364.

Jones, A. C., J. M. Haywood, N. Dunstone, K. Emanuel, M. K. Hawcroft, K. I. Hodges, and A. Jones, 2017: Impacts of hemispheric solar geoengineering on tropical cyclone frequency. *Nature Communications*, **8 (1)**, 1382.

Judt, F., R. Rios-Berrios, and G. H. Bryan, 2023: Marathon versus sprint: Two modes of tropical cyclone rapid intensification in a global convection-permitting simulation. *Monthly Weather Review*, **151 (10)**,

2683 – 2699.

Judt, F., et al., 2021: Tropical cyclones in global storm-resolving models. *Journal of the Meteorological Society of Japan. Ser. II*, **99**, 579 – 602.

Keys, P. W., E. A. Barnes, N. S. Diffenbaugh, J. W. Hurrell, and C. M. Bell, 2022: Potential for perceived failure of stratospheric aerosol injection deployment. *Proceedings of the National Academy of Sciences*, **119 (40)**, e2210036 119.

Khodri, M., et al., 2017: Tropical explosive volcanic eruptions can trigger el niño by cooling tropical africa. *Nature Communications*, **8 (1)**, 778.

Klotzbach, P. J., K. M. Wood, C. J. Schreck III, S. G. Bowen, C. M. Patricola, and M. M. Bell, 2022: Trends in global tropical cyclone activity: 1990–2021. *Geophysical Research Letters*, **49 (6)**, e2021GL095 774.

Knaff, J. A. and R. M. Zehr, 2007: Reexamination of tropical cyclone wind–pressure relationships. *Weather and Forecasting*, **22 (1)**, 71 – 88.

Knapp, K. R., H. J. Diamond, J. P. Kossin, M. C. Kruk, and C. J. Schreck, 2023: International best track archive for climate stewardship (ibtracs) project, version 4 [since1980].

Knapp, K. R., M. C. Kruk, D. H. Levinson, H. J. Diamond, and C. J. Neumann, 2010: The international best track archive for climate stewardship (ibtracs): Unifying tropical cyclone data. *Bulletin of the American Meteorological Society*, **91 (3)**, 363 – 376.

Knutson, T., et al., 2020: Tropical cyclones and climate change assessment: Part ii: Projected response to anthropogenic warming. *Bulletin of the American Meteorological Society*, **101 (3)**, E303 – E322.

Knutson, T. R., J. J. Sirutis, M. Zhao, R. E. Tuleya, M. Bender, G. A. Vecchi, G. Villarini, and D. Chavas, 2015: Global projections of intense tropical cyclone activity for the late twenty-first century from dynamical downscaling of cmip5/rcp4.5 scenarios. *Journal of Climate*, **28 (18)**, 7203 – 7224.

Kravitz, B., et al., 2013: Sea spray geoengineering experiments in the geoengineering model intercomparison project (geomip): Experimental design and preliminary results. *Journal of Geophysical Research: Atmospheres*, **118 (19)**, 11,175–11,186.

Lagouvardos, K., A. Karagiannidis, S. Dafis, A. Kalimeris, and V. Kotroni, 2022: Ianos—a hurricane in the mediterranean. *Bulletin of the American Meteorological Society*, **103 (6)**, E1621 – E1636.

Liu, F., J. Li, B. Wang, J. Liu, T. Li, G. Huang, and Z. Wang, 2018: Divergent el niño responses to volcanic

eruptions at different latitudes over the past millennium. *Climate Dynamics*, **50 (9)**, 3799–3812.

Lockley, A., Y. Xu, S. Tilmes, M. Sugiyama, D. Rothman, and A. Hindes, 2022: 18 politically relevant solar geoengineering scenarios. *Socio-Environmental Systems Modelling*, **4**, 18 127.

Mahfouz, N. G. A., S. A. Hill, H. Guo, and Y. Ming, 2023: The radiative and cloud responses to sea salt aerosol engineering in gfdl models. *Geophysical Research Letters*, **50 (2)**, e2022GL102 340.

McKay, D. I. A., et al., 2022: Exceeding 1.5°c global warming could trigger multiple climate tipping points. *Science*, **377 (6611)**, eabn7950.

Mueller, T. J., C. M. Patricola, and E. Bercos-Hickey, 2024: The influence of enso diversity on future atlantic tropical cyclone activity. *Journal of Climate*, **37 (15)**, 3959 – 3975.

Nardi, K. M., C. M. Zarzycki, V. E. Larson, and G. H. Bryan, 2022: Assessing the sensitivity of the tropical cyclone boundary layer to the parameterization of momentum flux in the community earth system model. *Monthly Weather Review*, **150 (4)**, 883 – 906.

Nayak, C., J. Bulusu, G. Vichare, and A. P. Dimri, 2024: Effects of solar variability on tropical cyclone activity. *Earth and Space Science*, **11 (6)**, e2023EA003 500.

NOAA, 2024a: Equatorial pacific sea surface temperatures (sst). URL `https://www.ncei.noaa.gov/access/monitoring/enso/sst`.

NOAA, 2024b: Hurricane damage potential. URL `https://www.noaa.gov/jetstream/tc-potential`.

NOAA, 2024c: Tropical cyclone climatology. URL `https://www.nhc.noaa.gov/climo/#:~:text=The%20official%20hurricane%20season%20for,%2DAugust%20and%20mid%2DOctober.`

Pezza, A. B. and I. Simmonds, 2006: Catarina: The first south atlantic hurricane and its association with vertical wind shear and high latitude blocking. *International Conference on Southern Hemisphere Meteorology and Oceanography (ICSHMO)*, Vol. 8, 353–364.

Randall, D. A., J. Hurrell, A. Gettelman, R. Loft, and W. Skamarock, 2019: Proposal to the National Science Foundation's Program for Cyberinfrastructure for Sustained Scientific Innovation for Collaborative Research: Frameworks: Community-Based Weather and Climate Simulation with a Global Storm-Resolving Model. URL `https://hogback.atmos.colostate.edu/earthworks/pdf/EarthWorks-proposal.enhanced.pdf`.

Richter, J. H., et al., 2022: Assessing responses and impacts of solar climate intervention on the earth system with stratospheric aerosol injection (arise-sai): protocol and initial results from the first simulations. *Geoscientific Model Development*, **15 (22)**, 8221–8243.

Roberts, M. J., et al., 2020: Projected future changes in tropical cyclones using the cmip6 highresmip multimodel ensemble. *Geophysical Research Letters*, **47 (14)**, e2020GL088 662.

Schurer, A., G. Hegerl, J. Luterbacher, S. Brönnimann, T. Cowan, S. Tett, D. Zanchettin, and C. Timmreck, 2019: Disentangling the causes of the 1816 european year without a summer. *Environmental Research Letters*, **14**, 094 019.

Smith, W. and G. Wagner, 2018: Stratospheric aerosol injection tactics and costs in the first 15 years of deployment. *Environmental Research Letters*, **13 (12)**, 124 001.

Sobel, A. H., A. A. Wing, S. J. Camargo, C. M. Patricola, G. A. Vecchi, C.-Y. Lee, and M. K. Tippett, 2021: Tropical cyclone frequency. *Earth's Future*, **9 (12)**, e2021EF002 275.

Studholme, J., A. V. Fedorov, S. K. Gulev, K. Emanuel, and K. Hodges, 2022: Poleward expansion of tropical cyclone latitudes in warming climates. *Nature Geoscience*, **15 (1)**, 14–28.

Tilmes, S., et al., 2018: Cesm1(waccm) stratospheric aerosol geoengineering large ensemble project. *Bulletin of the American Meteorological Society*, **99 (11)**, 2361 – 2371.

Tilmes, S., et al., 2020: Reaching 1.5 and 2.0 °c global surface temperature targets using stratospheric aerosol geoengineering. *Earth System Dynamics*, **11 (3)**, 579–601.

Tippett, M. K., S. J. Camargo, and A. H. Sobel, 2011: A poisson regression index for tropical cyclone genesis and the role of large-scale vorticity in genesis. *Journal of Climate*, **24 (9)**, 2335 – 2357.

Tory, K. J. and R. A. Dare, 2015: Sea surface temperature thresholds for tropical cyclone formation. *Journal of Climate*, **28 (20)**, 8171 – 8183.

Vitart, F., J. L. Anderson, and W. F. Stern, 1997: Simulation of interannual variability of tropical storm frequency in an ensemble of gcm integrations. *Journal of Climate*, **10 (4)**, 745 – 760.

Wallace, E. J. and S. G. Dee, 2022: Tropical cyclone frequency: turning paleoclimate into projections. *Environmental Research: Climate*, **1 (2)**, 023 002.

Walsh, K. J., et al., 2016: Tropical cyclones and climate change. *WIREs Climate Change*, **7 (1)**, 65–89.

Walsh, K. J. E., et al., 2015: Hurricanes and climate: The u.s. clivar working group on hurricanes. *Bulletin of the American Meteorological Society*, **96 (6)**, 997 – 1017.

Wang, H., et al., 2014: How well do global climate models simulate the variability of atlantic tropical cyclones associated with enso? *Journal of Climate*, **27 (15)**, 5673 – 5692.

Wehner, M. F., et al., 2014: The effect of horizontal resolution on simulation quality in the community atmospheric model, cam5.1. *Journal of Advances in Modeling Earth Systems*, **6 (4)**, 980–997.

Williams, I. N. and C. M. Patricola, 2018: Diversity of enso events unified by convective threshold sea surface temperature: A nonlinear enso index. *Geophysical Research Letters*, **45 (17)**, 9236–9244.

Zhang, Y., D. G. MacMartin, D. Visioni, and B. Kravitz, 2022: How large is the design space for stratospheric aerosol geoengineering? *Earth System Dynamics*, **13 (1)**, 201–217.

Zhao, M., I. M. Held, S.-J. Lin, and G. A. Vecchi, 2009: Simulations of global hurricane climatology, interannual variability, and response to global warming using a 50-km resolution gcm. *Journal of Climate*, **22 (24)**, 6653 – 6678.

APPENDIX

PHAST ALGORITHM

The Pressure-based Hybrid Algorithm for Storm Tracking (PHAST) represents a novel application of known empirical relationships between TC central pressures and wind intensity/category. Based in part on research directions suggested at the close of Davis (2018), and in light of the shortcomings of current GSRM's in representing storm intensity and convection (Judt et al. 2021), we have sought alternative means of quantifying modeled TC intensity distributions.

In the PHAST process, elements of the TSTORMS algorithm (Vitart et al. 1997; Zhao et al. 2009) are adjusted to account for high-resolution grid spacing (including the occurrence of storms close together in space), and paired with storm strength estimation using a wind-pressure relationship (WPR) adapted by Knaff and Zehr (2007) from work by Atkinson and Holliday (1977), with correction for storm intensity biases. Central TC minimum pressures (in hPa) at each time step are plugged into a form of this adapted WPR taken from Holland (2008) (equation 4):

$$V_{max} = 2.3(1010 - P_c)^{.76}$$

This relation yields equivalent maximum 1-minute sustained wind speeds. Thus, model outputs that represent real-world central TC pressures (P_c) more realistically than they do maximum wind speed (V_{max}), can yield TC tracking data with a more realistic range of storm categories.

The algorithm is implemented on (natively hexagonal) Earthworks outputs interpolated to a rectangular, .25° lat-lon grid. Variables are returned as instantaneous values given at 6-hour intervals, with the relevant fields comprising: 10M wind speed (U10); pressure at sea level (PSL); vorticity at 850 hPa height (vorticity850); and mean temperature between the 300-500 hPa pressure levels (T300-500). PHAST can be re-tuned to analyze data at other spatial and temporal resolutions as well.

The creation of storm tracks from variable fields by PHAST can be broadly divided into detecting candidate vortexes, stitching them together into trajectories, and filtering out extratropical cyclones and other edge cases, as outlined below.

With proximity defined as the greater of the difference in latitude or difference in longitude, in degrees, between two grid points:

(1) Candidate Vortexes

- At each time step, globally, scan for local vorticity850 maxima above threshold of 1.6×10^{-4} s^{-1}, with no other vorticity850 values higher within proximity 2 degrees.
- Find lowest PSL within proximity 2 degrees of vorticity maxima, the pressure center
- Find highest U10 value within proximity 2 degrees of pressure center
- Find the warm core center, the warmest individual T300-500 value within proximity 4 degrees of pressure center. There is only a valid candidate TC vortex when this highest temperature value is found within proximity 2 degrees of the pressure center, and is at least 1° C greater than the mean of the proximity 4 degree proximity box.
- Pressure centers arising from vorticity850, PSL, and T300-500 maxima/minima meeting these requirements are added to a list of vortex candidate positions, with accompanying properties, for the given time step.

(2) Making Trajectories

- Initialize two arrays, for dead_storms and living_storms.
- Load every candidate vortex from the first output time step into living_storms.
- For each subsequent time step, for every storm in living_storms, if there is a candidate vortex in the new time step within 400km, the storm continues on living, taking on the properties/position of the closest candidate vortex. Older living storms take priority

in being matched with candidate vortexes.
If two or more candidate vortexes are equidistant from a living storm, tie is broken by sum of how relatively northern and westward pressure centers are by degrees lat-lon.

- Living storms with no successor candidate vortex die, and are moved to dead_storms. Candidate vortexes unmatched with a current living storm become new living storms.
- At the end of each storm's lifetime, storm is identified as a valid TC if, on at least 3 model days, it achieved TS or TC intensity. For at least one time step on each of 3 days, the storm's direct model wind max must be at least 10 m/s, and WPR predicted wind max must be at least 17 m/s. Overall storm lifetime must be at least 72 hours.
- Storm category at each time step is based on WPR predicted wind max, plugged into Saffir-Simpson scale.

(3) Filtering Edge Cases

- To distinguish tropical storms from extratropical storms and other TC-like convective systems not a part of TC best track data, restrict valid storm tracks to those with pressure centers occurring over SST's of >=27° C for at least one time step. This does not exclude TC's later undergoing extratropical transition, but does exclude entirely continental/cold water systems from our consideration.